Heliyon 10 (2024) e25873

Contents lists available at ScienceDirect

Heliyon

journal homepage: www.cell.com/heliyon

Review article

Current significance and future perspective of 3D-printed bio-based polymers for applications in energy conversion and storage system

Khoiria Nur Atika Putri [a], Varol Intasanta [b], Voravee P. Hoven [c,d,*]

[a] Program in Petrochemistry and Polymer Science, Faculty of Science, Chulalongkorn University, Bangkok, 10330, Thailand
[b] Nanohybrids and Coating Research Group, National Nanotechnology Center (NANOTEC), National Science and Technology Development Agency (NSTDA), Pathum Thani, 12120, Thailand
[c] Department of Chemistry, Faculty of Science, Chulalongkorn University, Bangkok, 10330, Thailand
[d] Center of Excellence in Materials and Biointerfaces, Chulalongkorn University, Bangkok, 10330, Thailand

ARTICLE INFO

Keywords:
Energy conversion
Energy storage
3D printing
Bio-based polymers

ABSTRACT

The increasing global population has led to a surge in energy demand and the production of environmentally harmful products, highlighting the urgent need for renewable and clean energy sources. In this context, sustainable and eco-friendly energy production strategies have been explored to mitigate the adverse effects of fossil fuel consumption to the environment. Additionally, efficient energy storage devices with a long lifespan are also crucial. Tailoring the components of energy conversion and storage devices can improve overall performance. Three-dimensional (3D) printing provides the flexibility to create and optimize geometrical structure in order to obtain preferable features to elevate energy conversion yield and storage capacitance. It also serves the potential for rapid and cost-efficient manufacturing. Besides that, bio-based polymers with potential mechanical and rheological properties have been exploited as material feedstocks for 3D printing. The use of these polymers promoted carbon neutrality and environmentally benign processes. In this perspective, this review provides an overview of various 3D printing techniques and processing parameters for bio-based polymers applicable for energy-relevant applications. It also explores the advances and current significance on the integration of 3D-printed bio-based polymers in several energy conversion and storage components from the recently published studies. Finally, the future perspective is elaborated for the development of bio-based polymers via 3D printing techniques as powerful tools for clean energy supplies towards the sustainable development goals (SDGs) with respect to environmental protection and green energy conversion.

1. Introduction

The integral increase in human population translates to not only great demand for energy use but also enormous production of exhaustive products, which become the root cause of pollution. Hence, making the quest for renewable and clean energy sources is a never-ending battle for mankind. Continuous refinement on the energy conversion and storage systems has been made to increase the

* Corresponding author. Department of Chemistry, Faculty of Science, Chulalongkorn University, Bangkok, 10330, Thailand.
E-mail address: vipavee.p@chula.ac.th (V.P. Hoven).

https://doi.org/10.1016/j.heliyon.2024.e25873
Received 18 October 2023; Received in revised form 3 February 2024; Accepted 5 February 2024
Available online 11 February 2024

viability of clean and sustainable energy. Improvement of overall performance for energy conversion and storage could be achieved by tailoring the cellular component of the devices. Aiming for optimized geometries or assemblies that could increase the feasibility of respective reactions occurrence. Three-dimensional (3D) printing is the frontier method that offers rapid processing and limitless possibilities for creating and tuning morphological features of the desired material [1]. The computer-aided modelling prior to the printing process enables users to create intricate architecture layer by layer as per the need of material functionalities and end-use [2]. Therefore, such versatility makes this method suitable for a wide range of applications.

In energy conversion and storage, this method has been applied to fabricate several functional materials ranging from customized scaffolds for catalyst immobilization, microfluidic reactors, ion exchange membranes, electrodes and solid electrolytes [3–6]. These components are commonly tailored to have better mass transport by printing ion/compound diffusion channels, enhanced surface area in order to allow high loading of catalytically active materials, and alteration of the material surface to facilitate better interfacial mechanism by taking advantage of geometry freedom provided by 3D printing techniques [7–9]. Besides, the use of 3D printing in the manufacturing process also brings a chance to reduce operational costs due to the ability to precisely estimate the needed feedstock with the aid of computational modelling hence preventing the waste production [10]. Thus, it could be envisioned that 3D printing will be a solution to a sustainable large-scale manufacturing process for energy conversion and storage components in the near future.

In conjunction with sustainable manufacturing via 3D printing, considering the sustainability and ecology of the materials used in energy conversion and device fabrication is crucial. The major components in current energy conversion and storage devices were known to impose adverse impacts and potential threats to the natural ecosystem. This danger stems from the use of non-renewable and hazardous materials, which contributes to the depletion of natural resources and pollution of land and water ecosystems during their life cycle [11,12]. Therefore, it is imperative to undergo a paradigm shift by integrating bio-based materials in energy device components. Natural abundance, low toxicity, and degradability possessed by bio-based material shall promote sustainability and alleviate the environmental burden associated with energy devices [13].

Bio-based polymers, polymeric macromolecules sourced from biological or renewable resources, highlighted for their plentiful natural reserves, versatility, biocompatibility, and cost-efficiency, particularly pose as a sustainable and eco-friendly material alternative for energy application [14–16]. Their tunable macrostructure and high compatibility with other organic or inorganic materials made them excellent support for heterogeneous active materials in energy conversion and storage systems [17]. The macromolecular network and diverse chemical functionalities were also reported to facilitate ionic mobility, making them suitable as high-performing bio-inspired components for batteries, supercapacitors, and fuel cells [18]. Their inherent moieties and cost-efficiency also made them unique and economical carbon precursors in electrochemical energy conversion and storage systems [19]. Their ease of degradation contributes to a significantly reduced carbon footprint during disposal, thereby lessening the environmental impact associated with energy conversion and storage technologies [20]. Additionally, intrinsic physical properties, such as viscoelasticity and shear thinning behavior, made bio-based polymers processable through 3D printing techniques [21]. Therefore, this enables the feasibility of coupled advantages provided by 3D printing as customizable manufacturing technique, and the outstanding properties provided by bio-based polymers to obtain sustainable and efficient fabrication strategy resulting in high-performing energy conversion and storage devices.

Based on the aforementioned interest, this review will provide the current advances in using 3D printing techniques employing bio-based polymeric material to overcome systematical challenges in order to improve the overall energy conversion and storage system performance. The forthcoming discussion will also elaborate about the detailed properties and various fabrication strategy for integrating bio-based polymers into 3D-printed energy conversion and storage systems. Furthermore, this review will propose the future perspective while addressing current challenges of using 3D printing of bio-based polymer in energy conversion and storage systems as a fulfilling strategy to achieve Sustainable Development Goals (SDGs) regarding environmental protection and green energy conversion.

2. 3D printing of bio-based polymers for energy devices: techniques and post-printing treatment

2.1. 3D printing techniques and parameters

Layer-by-layer prototyping technique was first mentioned by Dr. Hideo Kodama in his research article dated in 1981 [22]. The evolution of 3D printing techniques began from his failed attempt to patent his innovation, allowing further development by the coming generations. Five years later, the concept of material prototyping based on photopolymerizable resin under ultraviolet (UV) light was patented by Charles W. Hull under the term of stereolithography (SLA). His patent included the use of a 3D model under the *.stl* file format and digital slicing method that later being used extensively prior to 3D printing process. In the following year, Hull also launched the first world-renowned 3D printer named the SLA-1 which made him the most credited innovator for the evolution of the 3D printing technique. Soon after, other 3D printing techniques were invented and currently classified into seven categories by the American Society for Testing and Material (ASTM) 52900. Their working principle, processable material, advantages and disadvantages of each technique are compiled in Table 1 while the workflow and simplified assembly are demonstrated in Fig. 1.

The use of bio-based polymers as a material for 3D printing has grown rapidly over the last decade, as indicated by the number of publications based on the Scopus database depicted in Fig. 2a. Interestingly, it was documented that the 3D-printed bio-based polymer material was developed for a wide range of applications ranging from medical to energy-related purposes (Fig. 2b). Several bio-based polymers categorized as polysaccharides, polyesters, polypeptides, polyphenols, and their derivatives (Fig. 2c) were favored due to their resource sustainability, cost-effectiveness, and versatility [16,23]. These polymers possess particular physical and chemical properties such as temperature sensitivity, degradation, viscoelasticity, and rheological properties, making them processable only by certain 3D printing techniques. Moreover, focusing on the application related to energy which often includes the need for the

Table 1
Summary of the classification, working principle, advantages, and disadvantages of various 3D printing techniques.

Classification	Printing Techniques	Material Feedstock	Working Principle	Advantages	Disadvantages
Vat Photopolymerization	Stereolitography (SLA)	Photocurable resins	The sequential layered structure is constructed through a concentrated photo-induced solidification process of the resin, utilizing either UV light or laser as the light source.	Smooth surface finish, easy scalability, able to produce intricate architecture.	Limited to one material processing at a time.
	Digital Light Processing (DLP)	Photocurable resins	The sequential layered structure is built up through the uniform photo-induced solidification of resin using a UV source. The wide coverage of the UV source spans across each layer, enabling rapid fabrication of the structure.	Large coverage of photocuring area inducing rapid processing compared to SLA.	Limited material feedstock, inefficient stepwise curing process.
	Continuous Liquid Polymerization (CLIP)	Photocurable resins	A continuous and simultaneous process of layer fabrication and photo-induced solidification occurs in CLIP. In this process, an oxygen-permeable membrane creates a "dead zone," enabling the continuous irradiation of photocurable resin by a light source while maintaining contact with the flowing resin beneath the built layer.	Simultaneous curing and dipping to UV resins makes the process faster.	Limited to single material processing.
Binder Jetting	–	Ceramics and metals-based powder.	The creation of layered structure based on the deposition of binder adhesive droplets in each printed layer of powdered ceramics/metal-based materials.	Room temperature processing, no support structure is required, high production rate.	Stepwise curing process requires, high surface roughness and low resolution in final product.
Directed Energy Deposition	–	Metals and wire source material.	The creation of layered structure based on the deposition of melted metal wires by lasers onto the printing platform.	Multi material processing, possible to fabricate large objects.	Low resolution, rough surface of final product, shrinkage and deformation could occur during processing due to differences in the temperature.
Extrusion	Fused Deposition Modelling (FDM)	Thermoplastics	The creation of layered structure based on the deposition of thermoplastic filaments that are heated above its glass transition temperature (Tg) allowing an extrusion process through the printing nozzle to the heated printing platform.	Simple and processing, inexpensive.	Often produce waste from the supporting parts of the printed object, post-printing treatment is necessary.
	Direct Ink Writing (DIW)	Viscous material, hydrogel, biomaterial	The creation of layered structure based on the extrusion process of viscous material aided by pneumatic air pressure of mechanical forcess. The viscous materials should possess a particular rheological and viscoelastic behavior to be able to form a mechanically stable structure during the printing process.	Room temperature processing, simple and versatile, high resolution printing.	Post-printing process (curing) is required.
Material Jetting	–	Photopolymers.	This method relies on the deposition of photopolymers droplets through tiny nozzles in the printhead to build the layers in the working object. The deposition process happens at the same time with the photocuring process	Able to print muti-materials and multicolored object.	Not suitable for large object fabrication, post-printing treatment is necessary.
Powder Bed Fusion	Selective Laser Sintering (SLS)	Thermoplastics and Metals.	This technique works based on fusing of powder material by laser or heat source to form the 3D scaffold. SLS process employed laser to sinter the powder material to create a solid scaffold.	Suitable for batch printing, no need of support structure, able to fabricate detailed final object.	Post-printing treatment is difficult, expensive, limited material feedstock.
	Selective Laser Merlting (SLM)	Metals	The SLM process employed laser as a heat source to melt the powder material to create a solid scaffold.	Able to fabricate detailed product.	Expensive
	Electron Beam Melting (EBM)	Metals	The SLM process employed electron beam as a heat source to melt the powder material to create a solid scaffold.	Produce less material waste, faster than laser sintering, no need of support structure.	Expensive, lower accuracy compared to laser sintering.
Sheet Lamination	Lamination Object Manufacturing (LOM)	Paper or sheet of metal, plastic, and laminated metals.	This technique works based on the pilling the raw material such as paper/sheet material in sequential layers to obtain the desired scaffold. Prior to the stacking of the sheets, adhesives are applied to induce bonding between two successive layers. Then, laser beam is used to weld the materials to create the desired contour.	Fast and inexpensive for the fabrication of large objects.	Rough surface in the final product, difficulties in final product separation, there are complications in producing internal structures.

(–) sign indicated that 3D printing classification is directly associated with printing technique without any variation in the workflow.

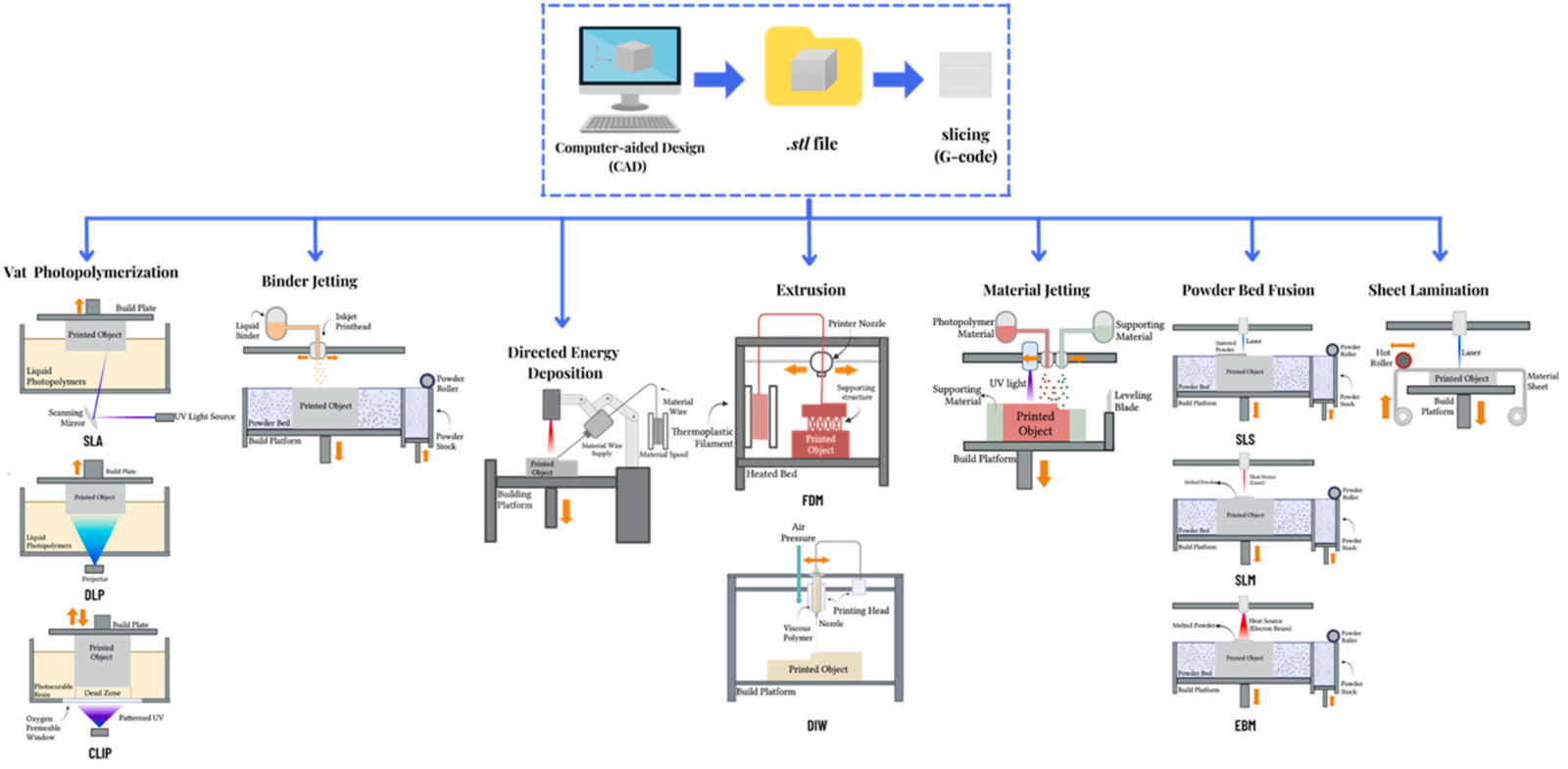

Fig. 1. Workflow and simplified schematic assembly of 3D printing techniques as classified by ASTM.

incorporation of several additives (i.e., catalyst, ionic salts, and sacrificial inorganic particles) in the ink formulation, making the extrusion-based 3D printing the most suitable technique for bio-based polymers [24].

In extrusion-based 3D printing, several aspects, such as rheological and printing parameters, should be optimized to obtain a printed structure with high fidelity and mechanical stability (Fig. 3). The basic rheological requirement for a material to be useable as ink is that it should be a viscous homogeneous fluid that can deposit smoothly without causing nozzle clogging. Its viscosity should be low under a high shear rate caused by the applied pressure from the printer to allow the ink to flow out of the nozzle. Then after the ink is deposited, it should instantly regain its solid-like characteristic to retain its shape [25,26]. Bio-based polymers, typically long-chain macromolecules built by covalently bonded monomeric units bearing diverse chemical functionalities enabling intermolecular interactions resulting in chain entanglement, are appropriate material complying with the 3D printing ink requirement [27]. The presence of chain entanglement caused by intermolecular hydrogen bonding, ionic interactions, and van der Waals forces results in the viscoelastic response of the polymer fluids under applied force. The understanding of bio-based polymer viscoelasticity directly correlates to its flow behavior upon extrusion in 3D printing process. Initial assessment for the bio-based material printability could be done based on visual inspection of the ink upon extrusion. The formation of filaments instead of droplets was related to the ability of

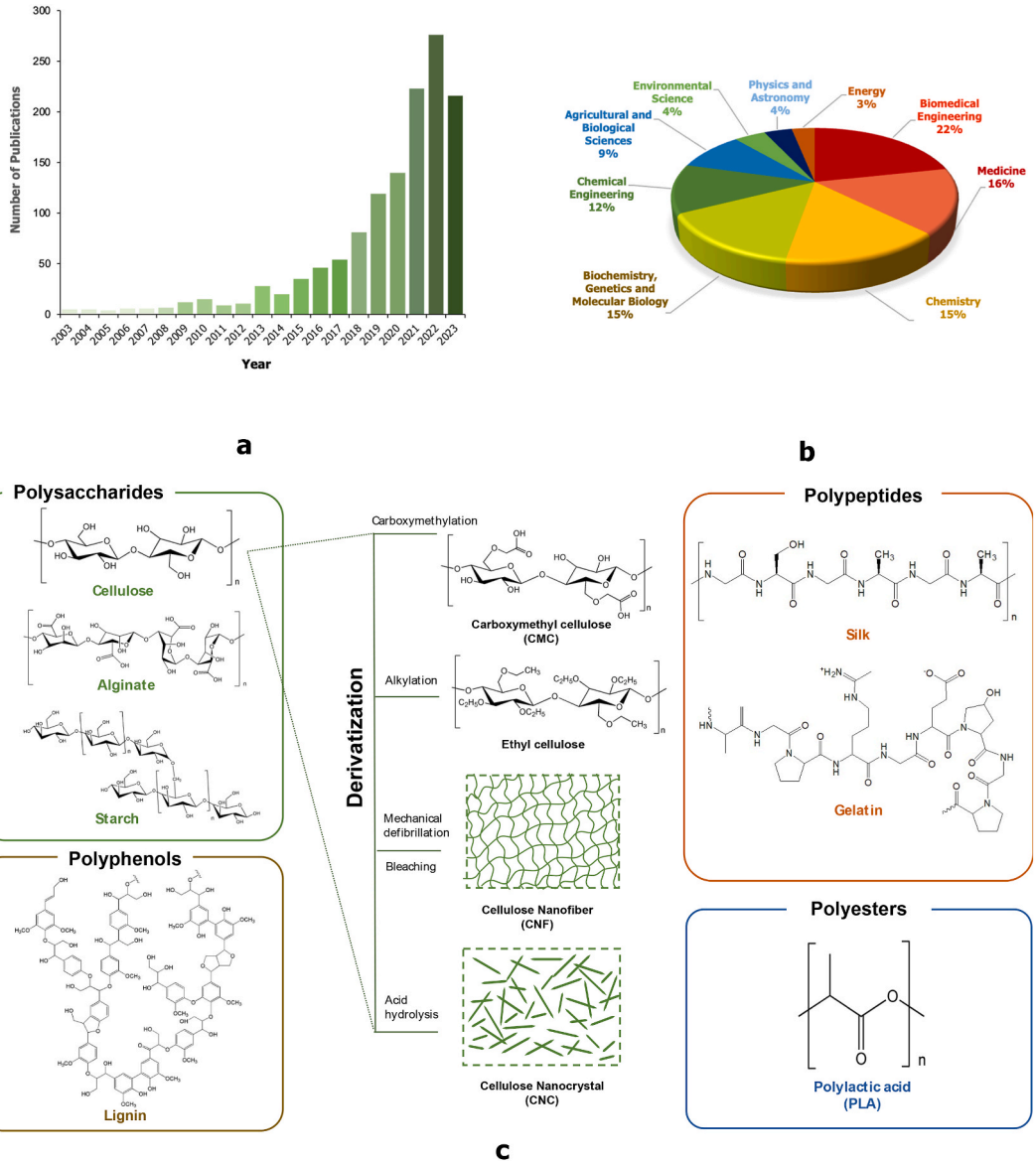

Fig. 2. Statistical representation on the use of bio-based polymers as materials in 3D printing processes based on (a) a number of publications per year and (b) applications by field. The data are generated from Scopus database on July 2023 by using the keywords of "3D printing", "bio-based polymer","biopolymer", "3D print bio-based polymer", and "3D print biopolymer" with manual exclusion of irrelevant data and (c) several 3D-printable bio-based polymer classes.

the material to deform under applied shear force upon extrusion, inducing flow imitating viscous liquid and quickly recovering its elastic response to maintain the filamentous shape integrity [28].

The comprehensive assessment of bio-based material printability should be based on its rheological parameters. Rheology is material deformation behavior under an applied force [29]. The intermolecular chain entanglement of bio-based polymers creates internal frictional forces that hinder the movement of polymeric chains upon experiencing external forces. This internal resistance to deformation is quantified as viscosity [27]. This polymeric chain conformation is very susceptible to deformation affected by applied external forces. Shear force is one of the determinants of polymer fluid flow and viscoelastic response. There are two types of material deformation behavior under applied shear force: Newtonian behavior and non-Newtonian behavior. Material's behavior would follow the Newtonian law when the viscosity is independent of shear force. Meanwhile, when the viscosity becomes higher or lower due to applied shear force, the material is said to be non-Newtonian, having shear thickening and shear thinning behavior, respectively [30,31]. The elastic and viscous response of polymers is represented as storage (G') and loss modulus (G"), respectively. At low shear rates, the chain entanglement of the bio-based polymers tends to restrict the chain movement resulting in high apparent viscosity, thus showing an elastic solid-like behavior ($G' > G''$). As shear rates increase, surpassing the yield stress point (τ_y), where $G' = G''$, disentanglement and chain reorientation to the bio-based polymer chain following the direction of applied forces start to happen [32]. The polymer chain disentanglement caused the apparent viscosity reduction and led to viscous flow behavior ($G' < G''$). Through this mechanism, a polymeric material is said to exhibit shear-thinning properties, which in the 3D printing process explains the extrudability and flow behavior of ink through the printing nozzle. The ratio between both values (G''/G') is defined as loss tangent (tan δ) which could be used to determine whether or not the polymeric ink is suitable for the extrusion-based printing process. Ink material with the tan $\delta > 1$ value and defined to be dominated by its viscous behavior can be easily extruded during printing. The polymeric material with tan $\delta < 1$, should be dominated by a solid-like elastic behavior [33,34].

Ma et al. have reported that the rheological behavior of the cellulose nanocrystal (CNC) was highly dependent on the concentration. Analyzed by using an oscillatory rheometer, the CNC having a concentration lower than 10 wt% showed a viscous behavior ($G'' > G'$), which made the hydrogel not printable as it could not retain its shape after being extruded from the printing nozzle. However, when the CNC concentration was increased from 10 to 25 wt%, it showed adequate elastic behavior, indicating that in this range, the hydrogel is printable using the direct-ink writing (DIW) technique and resulting in good shape retention. However, the high viscosity and yield stress of the hydrogel in this range may require a printer that could generate high pressure [35]. Another external factor affecting bio-based polymer rheology is temperature. Kokol et al. observed the temperature dependency of gelatin rheological behavior in the 3D cryo-printing process. The G' and G'' value of the material was significantly increased when the temperature was lowered and found to be decreased when temperature was elevated [36].

In order to be able to maintain the extruded shape, quick chain relaxation upon the removal of the shear force during the end of the extrusion process is necessary. The relaxation on the bio-based polymer chain led to the increment of its apparent viscosity. It brought back the domination of its elastic response, leading to the ability of the extruded bio-based polymers to maintain its filamentous shape. The time dependency on the change of bio-based polymer apparent viscosity described in the above mechanism is termed thixotropic behavior. Li et al. investigated the change in alginate hydrogel viscosity upon printing by extrusion-based technique, which was lowered as the shear rate was increased. The alginate hydrogel ink was observed to be able to regain its mechanical strength after being dispensed through a printing nozzle, demonstrating excellent thixotropic behavior of bio-based polymers [37].

Other than the rheological and mechanical properties of the bio-based ink, optimization towards printing parameters is also important to obtain 3D scaffold with high resolution. The parameters under this review scope include nozzle diameter, nozzle height, printing speed, and printing pressure. Nozzle diameter in extrusion-based 3D printing directly dictates the resolution of the printed scaffold. A small diameter would yield fine printed filament to give higher resolution to the printed scaffold. However, small diameter of the nozzle opening is very vulnerable to clogging which may make it unsuitable for certain ink formulations. On the contrary, a large nozzle diameter would promote smooth ink extrusion but may result in a rougher printed scaffold [38]. Czyżewski et al. investigated the effect of different nozzle size for the printing of PLA using FDM techniques. The diameters of 0.2, 0.4, 0.8, and 1.2 mm were used to print a 3D scaffold with 0.2 mm layer height and 100% infill. It was found that the use of 0.8 mm nozzle diameter promotes high degree

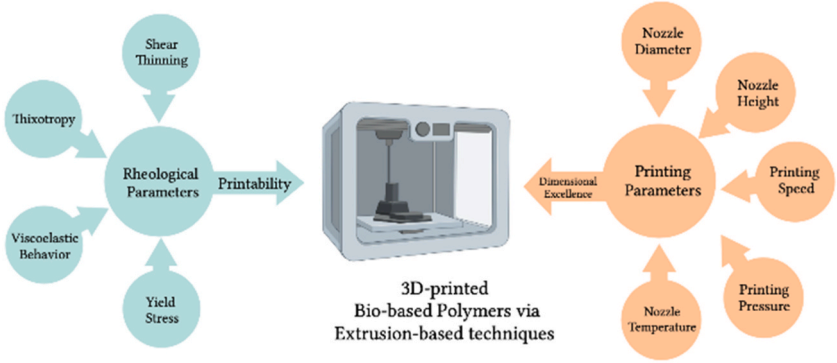

Fig. 3. Physical properties and processing parameters for 3D-printed bio-based polymers via extrusion-based techniques.

of interconnection of printed layers thus promoting better mechanical properties [39]. Brandley et al. reported the use of ultra-fine nozzle diameter of 10 and 30 μm to print carboxymethyl cellulose (CMC) using DIW technique. The printing process was possible without any clogging due to the aid from the elastic properties of CMC in high concentration. The possibility to print CMC using ultra-fine nozzle enables the opportunity for detailed fabrication of 3D scaffold in micro and meso scale [40]. Li et al. reported the relation between nozzle diameter and printing pressure. It was deduced that the smaller nozzle diameter would require higher printing pressure for printing via the DIW technique [41].

Aside from the diameter, the height of the nozzle during the printing process also played a role in the dimensional fidelity of the printed scaffold. It was investigated that high distance of the nozzle to the platform resulted in smaller extruded filament during the printing, as mathematically presented in Eq. (1):

$$h_c = \frac{V_d}{\upsilon_n D_n} \tag{1}$$

which h_c is optimal nozzle height (mm), V_d is volume extrusion rate (cm^3/s), υ_n is nozzle moving speed (mm/s) and D_n is nozzle diameter [42].

It was previously found that, inadequate nozzle height resulted in squashed filaments. While wide distance between the nozzle and the building platform led to the broken printed filament [28]. It was described by He et al. that the nozzle height of less than 0.4 mm for sodium alginate (SA) and gelatin ink printing resulted in a sharp angle in the printing scaffold. When the nozzle height was increased, a curvy corner was observed. This phenomenon relates to response lag when the printing nozzle height is not properly tuned [43].

Extrusion rate is another important factor affecting the printability of bio-based ink in relation to the change of surface tension affected by viscosity. Polymeric ink material possessing shear thinning behavior have lowered viscosity when extruded in high extrusion rate, hence results in high surface tension. This phenomenon results in the smooth surface of the extruded filament. The correlation between viscosity and surface tension is empirically described in Eq. (2).

$$\gamma = A_{experimental} \bullet B/\eta \tag{2}$$

where A and B are the dimensional constants specific to each compound of interest while γ and η represent the values of surface tension and viscosity, respectively [44,45].

It is also known that extrusion rate should be optimized along with the printing pressure in the extrusion-based printing techniques. High printing pressure combined with high printing speed result in extruded ink in droplet form instead of filament. While low printing pressure with low speed would result in thick printed filament. Thus, the balance between both parameters must be optimized [46].

Additionally for extrusion-based printing techniques employing thermoplastic materials, the knowledge related to the glass transition temperature (T_g) is necessary. *Tg* is the temperature region in which the polymer chain exhibited molecular mobility due to the introduction of heat. The chain mobility resulted in the change of polymers from "glassy" solid state to "rubbery" molten state [47,48]. In 3D printing process of FDM, the increment of temperature would increase the fluidity of the extruded thermoplastic filament. Improper temperature adjustment will result in 3D printed structural dimension deviation and rough surface [49].

2.2. Post-printing treatment

The fabrication of energy conversion and storage systems featuring bio-based polymer through the 3D printing process often necessitates certain properties such as excellent mechanical stability, high surface area, adequate ion diffusion channels, and electrical conductivity. Thus, requiring particular post-printing treatment for the pristine bio-based polymers prior to application as summarized in Fig. 4. The most crucial post-printing treatment for bio-based polymers is solidification. The solidification strategy should refer to the desired final properties. It may vary from conventional ambient temperature drying to crosslinking processes. Thermoplastics, such as PLA, in which the solidification of the printed structure relies on the temperature difference between the nozzle, printing platform, and ambient temperature. In a recent report in which a complete assembly of lithium-ion battery including electrodes, current collector, and device case was fabricated employing PLA via FDM technique, the desired structure was obtained directly after the complete deposition of melted polymer. The extruder nozzle temperature was set at 210 °C to ensure the printability of PLA filament, while the printing platform temperature was set at 60 °C. The printed structures of the battery were then collected once it reached room temperature and used as a scaffold for the Li-salts electrolyte without further modification [50]. A supercapacitor electrode fabricated by PLA-graphene filament via FDM technique. The PLA/graphene filament was extruded with nozzle temperature of 220 °C with no adjustment to printing bed temperature. The printed structure was solidified by letting it cooled down to room temperature [51].

Crosslinking is the most common post-printing solidification process for bio-based polymers that do not undergo instant drying at ambient temperature. A flexible supercapacitor electrode and electrolyte fabricated from alginate were reported to undergo chemical crosslinking in the presence of calcium ions (Ca^{2+}) which not only solidified the printed structure but also initiated unique interaction between two printed parts. The alginate in both electrode and electrolyte was found to form bridged interaction linked by the Ca^{2+} present in the interphase. This chemical interaction was reported to promote excellent mechanical strength and electrode-electrolyte interfacial contact, thus elevating supercapacitor performance [52].

In certain applications, the printed structures were expected to possess porous structure. It could be easily achieved by the fabrication of aerogel through freeze drying/casting. A porous supercapacitor electrode based on cellulose nanofiber (CNF) was prepared by freeze-drying the 3D-printed hydrogel. After the complete deposition of CNF hydrogel, the printed structure was frozen at

−4 °C prior to the freeze-drying process for 48 h to remove water. This fabrication strategy resulted in randomly interconnected fibrous structures forming microporosity due to the sublimation of ice crystals. The overall structure possessed low density and high porosity of 0.189 g cm^{-3} and 87.38%, respectively. The CNF aerogel modification via *in situ* polymerization of polyaniline (PANI) made this material applicable as electrodes in supercapacitors. It was described that the porosity induced by the post-printing via freeze-drying process increased the surface area accessible for electrolyte transport, thus accelerating ion diffusions [53]. Another strategy for fabricating hierarchically porous supercapacitor electrodes based on cellulose aerogel was reported by combining the ability of 3D printing with freeze-drying as a post-printing treatment, leaching of sacrificial porosity agent, and chemical treatment. A viscous ink comprised of silicon dioxide (SiO_2) and CNC was printed using DIW techniques. After the complete grid lattice structure with micron-sized pores was printed, the hydrogel was kept refrigerated at −20 °C and subjected to freeze-drying process under vacuum, leaving micropores from the sublimed ice crystal. The SiO_2, a sacrificial hard template to form mesopores, was leached using sodium hydroxide. Further chemical treatment employing potassium hydroxide was done to induce nanopores. This multiscale porosity has proven to provide ion diffusion channels with low tortuosity leading to the increment of capacitance performance [54]. It was often that relying only on freeze-drying to create porous 3D printed bio-based polymer lattices resulted in mechanical instability due to immense shrinkage in the inner microstructure of material. The combined fabrication strategy via chemical crosslinking, freeze-thawing, solvent exchange, and ambient drying was proposed to yield a mechanically stable and porous structure for supercapacitors. A 3D printed 3D grid lattice derived from alginate and CNF was incorporated with divalent metal ion salts ($CaCl_2$) to form a semi-crosslinked pre-gel as ink for 3D printing. The presence of the crosslinking process prior to 3D printing was expected to minimize the shrinkage during the ice templating process executed by the freezing and thawing process. The printed structure was completely solidified after a solvent exchange process from ethanol to acetone, followed by air drying at room temperature. This strategy resulted in an aerogel with a continuous lamellar structure and low shrinkage, leading to mechanically stable material under compression force. The porous structure formed during the ice templating has also been found to elevate electrolyte diffusion in supercapacitor assembly [55].

Additional treatment for the 3D printed bio-based polymer after solidification might be necessary for it to be applicable in energy conversion and storage system. Thermal treatment is the most commonly used fabrication strategy after solidified 3D printed bio-based polymer has achieved. Through thermal treatment, bio-based polymers could be eliminated or converted into carbonaceous compound thus minimizing its undesirable electrical resistivity. A thermal treatment under nitrogen (N_2) atmosphere at 350 °C for 3 h has proven to elevate the electrical conductivity of 3D printed PLA/graphene and PLA/carbon electrodes. Other than that, thermal treatment was also proven to preserve fine-printed structure. The thermally treated 3D printed electrodes was reported to have faster electron transfer compared to untreated and chemically treated ones [56]. Complete elimination of electrical insulating PLA was also demonstrated by heating at 300–500 °C under air atmosphere. The increment on heating temperature was reported to yield less PLA residues and affect the capacitance value performance [57]. Thermal treatment could also be used to reduce a compound in the ink material. A pseudo

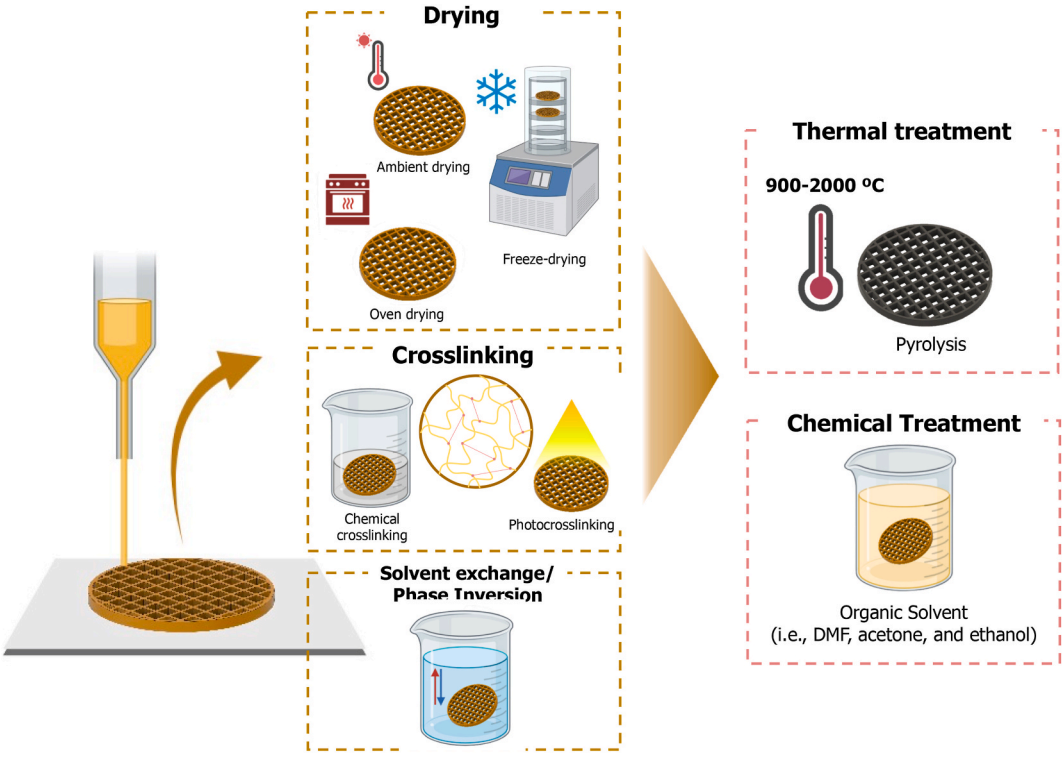

Fig. 4. Various post-printing treatments suitable for bio-based polymer in energy devices fabrication.

capacitor electrode based on 3D printed hydroxypropyl methyl cellulose/graphene oxide (HPMC/GO) aerogel underwent thermal reduction at 1050 °C under N_2 atmosphere for 3 h to form graphene aerogel. The reduction of GO to graphene has reported to promote better electrical conductivity of the material [58].

Chemical treatment is also an option as a post-solidification treatment for bio-based polymers applied in energy system. This strategy is often used to eliminate the undesired properties of bio-based polymers. The effect of solvent treatment using DMF was investigated on the electrochemical performance of PLA/graphene electrode. Immersion in DMF for 10 min has reported to cause physical spalling of PLA. The elimination of PLA by DMF has promoted better electron transfer thus elevating the electrochemical performance when applied in hydrogen evolution reaction system [59]. Other solvents such as acetone, ethanol, methanol, and water effect on the electrochemical performance of PLA/graphene 3D-printed electrode was also investigated. It was found that electrodes treated in polar aprotic solvent experienced dramatic increase in heterogeneous electron transfer and showed longer discharge profile in the energy storage system [60].

3. 3D printing of bio-based polymers in energy conversion system

Several strategies to produce a cleaner alternative to fossil fuels via environmentally benign processes have been extensively investigated. Several methods, such as catalytic energy conversion with the aid of photon, electrical current, and microbial metabolism, have been highlighted due to their high efficiency, ability to produce high-purity compounds, minimum production of harmful byproducts, and utilization of sustainable driving forces [61–63]. These processes enable the conversion of naturally abundant compounds such as water, carbon dioxide (CO_2), and nitrogen into hydrogen (H_2), methane (CH_4), and methanol (CH_3OH), which are potential alternative fuel compound [64]. Current challenges to these technologies include the attempt to elevate the conversion performance by focusing on the morphological modification to promote conversion reactants (i.e. ions, analyte, and photon) and also lower the capital cost of the device component fabrication through cost-efficient manufacturing using inexpensive raw materials [24, 65]. The attempt to overcome these challenges by tailoring the geometry by using 3D printing employing bio-based polymers will be elaborated in the following sections.

3.1. 3D-printed matrix for catalytic energy conversion

Energy conversion utilizing a suspended catalytically active material in an aqueous system has been favored due to its effectiveness owing to the superior surface area of the material and the simplicity of the reaction system. However, material retrieval upon the end of the conversion process often meets technical complications. It potentially leads to the generation of secondary pollutants in case of incomplete material separation. Considering these difficulties, the immobilization strategies for catalytically active materials are continuously innovated by fabricating thin films, sheets, and gels, which provide practicality for use. However, this kind of bulk structure often suffers from the inhibited transfer of the reaction driving forces (i.e., mass, photon, or heat) that could possibly lead to

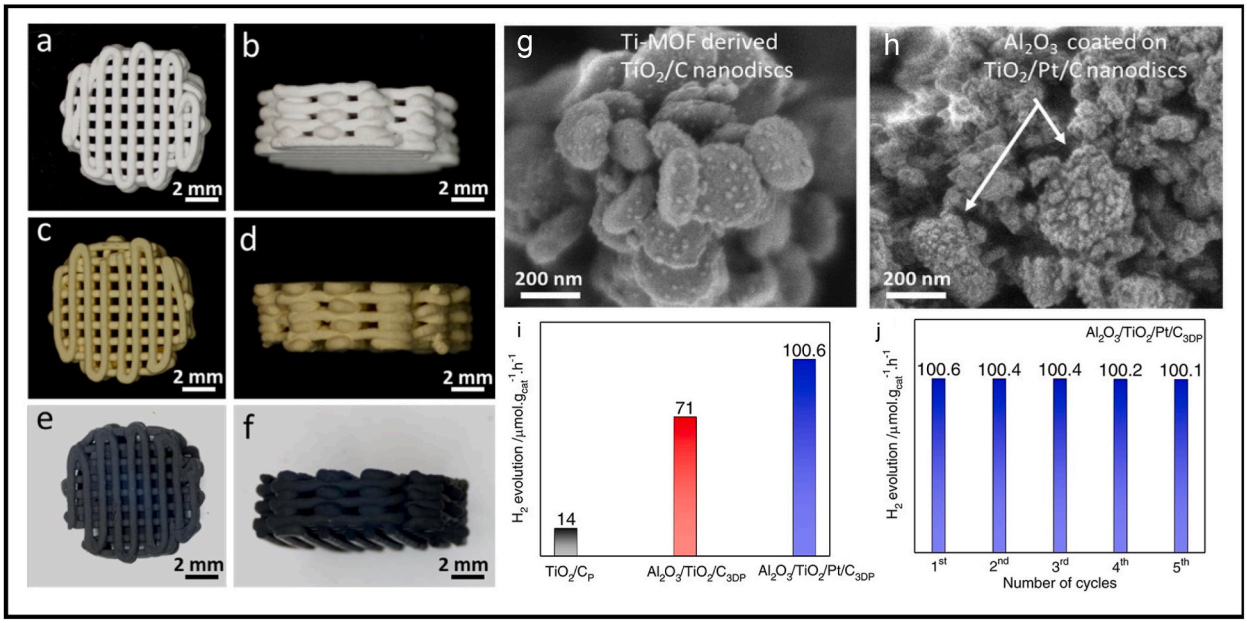

Fig. 5. The 3D-printed monolith of (a, b) boehmite (c–d) boehmite/Ti-MOF, (e–f) pyrolyzed $Al_2O_3/TiO_2/Pt/C$; SEM image of (g) Ti-MOF-derived TiO_2/C and (h) Pt-deposited boehmite/Ti-MOF-derived $Al_2O_3/TiO_2/Pt/C$; (i) HER activity of the samples and (j) reusability of 3D-printed $Al_2O_3/TiO_2/Pt/C$. Adapted from Ref. [67] licensed under CC-BY.

the reduction of conversion efficiency [66].

In an attempt to overcome these issues, 3D printing is recently highlighted due to its capability to construct a 3D matrix to anchor the catalysts and photocatalysts, facilitating the transfer of reaction-driving forces, thus presenting a high conversion yield. A 3D monolith of Titania-based metal-organic framework modified wilt aluminum oxide (Al_2O_3) as presented in Fig. 5a–h. The 3D-printed structure showed superior hydrogen production capability up to five times higher compared to its powder counterparts (Fig. 5i,j). The optimized 3D structure allowed the formation of micro- to nanopores that facilitated the mass transfer of the aqueous solution during the conversion process. The designed architecture also allowed better penetration of photons, hence enabling maximum exposure to the photocatalytic active material. This photon accessibility leads to the increment of hydrogen evolution performance [67].

The 3D printing techniques also been reported to fabricate dual functional material for ethylene production from CO_2. It was used to tune the porosities of the fabricated monolith to possess excellent CO_2 adsorption capacity. While the ink consisted of zeolite (ZSM-5) as catalyst immobilized in a 3D-printed monolith derived from metal-doped (Ce, Mo, Cr, and In) metal oxide (CaO) bound with a mixture of bentonite, calcium carbonate ($CaCO_3$), and methyl cellulose was catalytically active to convert CO_2 into ethylene. Methyl cellulose was used to regulate the 3D printability to yield on fine 3D structure. Through geometrical and composition optimization to achieve dual functionalities of adsorption and catalytically active sites, the obtained highest conversion percentage was 33.8% [68].

3.2. Microbial fuel cell

Microbial fuel cell (MFC) is a bio electrochemical system being able to perform conversion of chemical into electrical energy by employing microbial electroactive species as the main driving force. Microbial activities in MFCs electrode caused an oxidation to the substrate yielding electrons in the process. The electrons were then absorbed in the anode as an artificial electron acceptor to be further transported to the cathode facilitating the energy generation [69]. The fabrication of MFC component using 3D-printed bio-based polymer is currently highlighted. Recently, the fabrication of a cathode derived from the 3D-printed alginate was demonstrated using extrusion-based printing technique. Alginate was chosen as an alternative binder to commercial polytetrafluoroethylene (PTFE) due to its versatility, cost efficiency and high modulus. Its biodegradability is also an attractive feature so that this cathode could have lower environmental impact when compared to PTFE. It was reported that the alginate-based electrode possessed superior power levels of 286 μW and could be manufactured within a short period of time (45 s) via the DIW printing technique [70]. PLA was reported to be used for the fabrication of both cathode and anode for membrane-less MFC (Fig. 6a–h). Surface modification by coating using graphite and nickel was performed to enhance the conductivity. It was found that the carbon-coated PLA anode has peak power of 376.7 μW meanwhile the cathode has very low power. Its excellent ability to power source in digital weather station was demonstrated in Fig. 6i. In this case, the 3D printing technique was employed to reduce overall production cost and flexibility in structural fabrication of membrane-less assembly [71]. The use of 3D-printing method for the production of detailed structure up to 9.7 cm^2 on PLA electrode was demonstrated. This electrode was reported to have power density value of 14.6 mW [72]. Another notable example of MFC component fabricated from 3D-printed bio-based polymer along with their performance are listed in Table 2.

3.3. Electrolyzer and photoelectrolyzer

Energy conversion through electrochemical reactions has recently employed for its potential to yield electricity and fuel compounds. Through consecutive half reaction of HER occurs in the cathode and OER in anode of a fuel cell, H_2O could be converted into H_2 that could be utilized as cleaner alternative to fossil fuel via reaction mechanism shown in Eq. (3).

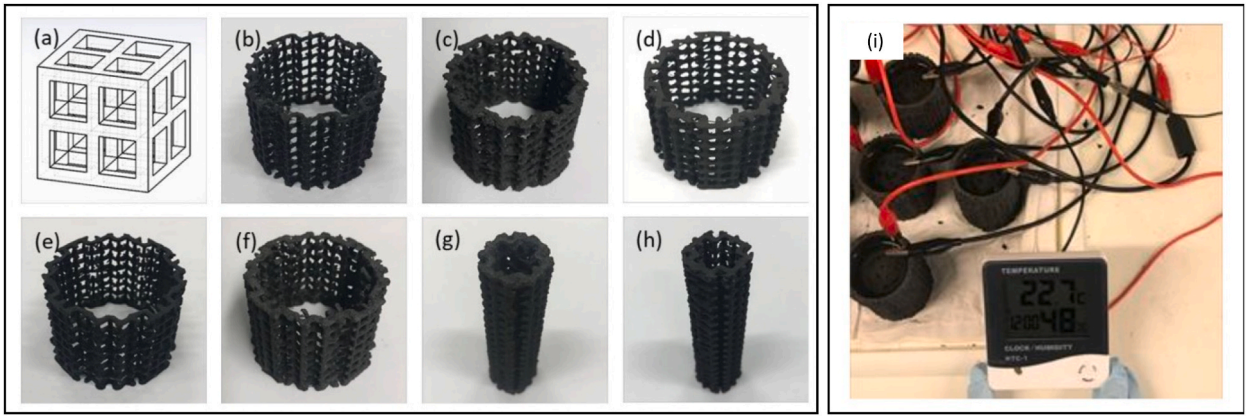

Fig. 6. The (a) 3D design of electrode, (b) PLA anode, (c) carbon-coated PLA anode, (d) Ni-coated PLA anode, (e) conductive PLA anode, (f) carbon-coated conductive PLA anode, (g) carbon-coated PLA cathode, (h) Ni-coated PLA cathode for microbial fuel cell, and (i) demonstration on the use of microbial fuel cell as a power for digital weather station. Reproduced from Ref. [71]. Licensed under CC-BY.

Table 2
Various MFC component fabricated from 3D-printed bio-based polymers and their performance.

Bio-based Polymer	3D Printing Technique	3D-printed Structure and Component	Microorganism	Performance	Significance	Ref.
Alginate	DIW	Monolith for cathode.	Microorganism from sewage sludge and urine.	$P_{max} = 286\ \mu W$	The 3D printing was used for rapid manufacturing strategy to produce MFC electrodes. The use of alginate was used as a substituent for toxic polytetrafluoroethylene (PTFE)-based component. Alginate was also calculated to lower the capita; production cost.	[70]
Alginate and cellulose	DIW	Grid patterned rectangle for anode	Shewanella Oneidensis MR-1.	$P = 3.5$ W/m	The 3D printed structure enhanced the electrolyte-accessible surface area. The use of alginate and cellulose aided the success in the integral printing of living bacteria.	[73]
PLA	FDM	Cuboid for anode	Microorganism from sewage sludge.	$P_{max} = 43 \pm 1\ \mu W$	The 3D printing was used to tune the porosity of the membrane to prevent analyte lost.	[74]
	FDM	Rectangular shape for cation exchange membrane.		$P_{max} = 240 \pm 11\ \mu W$	The optimized design rationale for the anode was also obtained. The PLA-based component fabricated via FDM techniques was favorable for its rapid and cost-efficient manufacturing ability.	
PLA	FDM	Basket-like structure for electrode.	Microorganism from sewage sludge.	$P_{max} = 376.7\ \mu W$	The 3D printing was used as rapid manufacturing strategy for the fabrication of membrane-less MFC assembly.	[71]
PLA	FDM	Rod and spirals shape for electrode.	Microorganism from cheddar and Feta Cheese wastewater.	*Current density* = 1.5 mA/cm^2 at 2 V	The fabrication of electrodes in microbial electrolysis for H_2 production in spiral shape allow better flow of H_2 bubble in the electrolyte system. The tuned number of spirals in electride geometry allow the prevention of produced H_2 gas bubble between the electrode surface.	[75]
PLA	FDM	Rectangular shape for electrode and MFC chamber (single and double).	Bacteria from compost.	$P = 18.6$ mW	PLA was chosen due to its biocompatibility to fabricate the whole MFC assembly. 3D printing was employed due to its significance to fabricate customizable single and double-chambered MFC.	[72]
Cellulose	DIW	Rectangular biofilm for cathode.	*Sporomusa Ovata.*	n/a	The 3D printing was used to tune the surface-to -volume area of the film electrode. Cellulose was used as a biocompatible material that could promote dense growth of the microorganism, hence increasing the electron production within the MFC system.	[76]

P_{max} is a symbol for peak power produced by the MFC component while P represents the power density generated per area of the MFC component.

$$\begin{array}{lll} HER: & H_2O + 2(h^+) \rightarrow & 1/2\ O_2 + 2H^+ \\ OER: & 2H^+ + 2e^- \rightarrow & H_2 \\ H_2o & \rightarrow & 1/2\ O_2 + H_2 \Delta G = 237.2\ KJ/mol \end{array} \quad (3)$$

In the presence of CO_2, the transfer of electrons in the anode could be used to induce the CO_2RR resulting in C1 (e.g., carbon monoxide (CO), formic acid (HCOOH), methanol (CH_3OH), formaldehyde (HCHO), and methane (CH_4)) and C2 (e.g., ethylene (CH_2CH_2), ethanol (C_2H_5OH), and acetate (CH_3COOH) products which could be further used as fuel feedstocks. If a photo-active material is employed, the system is termed as photoelectrolyzer [29,77,78].

This system has recently adopted the use of 3D-printed bio-based polymer to enhance the reaction efficiency by tuning the morphological properties of its components. Several advantages of morphological alteration via the 3D printing process, such as enhanced electrolyte permeability, optimized surface area, and elevated photon absorption, were reported. PLA/graphene composite filament is currently being extensively used for this application. This filament, later commercialized under trade name of Black Magic, is commonly processed using FDM printing technique to obtain the 3D-printed electrodes. In addition, the use of bio-based polymers in photo- and electrocatalysis systems is advantageous in terms of resource sustainability, cost-efficiency, and eco-friendliness. These parameters are directly related to the scalability of the component fabrication. Bio-based polymers with various chemical functionalities are also viable to serve as a support for photo- and electrocatalyst through H-bonding, electrostatic interaction, and metal-chelate complex formation. Such chemical interactions were reported to provide desirable conditions for uniform-size formation and dispersion of the catalytically active materials [17]. Besides that, combined with post-treatment processes such as pyrolysis, several bio-based polymers containing natural impurities (PLA), nitrogen (chitin, chitosan, and lignin), and sulfur (keratin) were reported to serve as excellent carbon-based catalyst and electrode material. These inherent properties act as a dopant or catalytic active sites for photo- and electrochemical conversion processes [19,79].

The presence of naturally embedded impurities adhered to the PLA/graphene filament that may affect its catalytic activity was reported. Ti and Fe impurities were reported to be found in PLA/graphene filament. However, these impurities have led to good HER activity. In term of PEC water splitting, the 3D-printed electrode fabricated from PLA/graphene could have great photocatalytic activity as the metal impurities may act as photocatalyst, i.e., TiO_2 and Fe_3O_4, after thermal post-printing process. This process can also convert PLA into graphitic carbon upon annealing in inert atmosphere which increases the conductivity of the electrode. In addition, solvent treatment by DMF was reported to cause swelling and physical spalling of PLA thus exposing the Ti and Fe impurities. These post-printing treatment were reported to enhance the HER activity as compared to the untreated PLA/graphene filaments [80]. Post-treatment using saponification method was described to successfully reduce the resistance of 3D-printed PLA/graphene composite. The saponification was done through hydroxide soaking process or through water electrolysis which gave similar results. It was proposed that the saponification treatment by electrolysis had significantly improved the electrode accessibility without exposure to hazardous caustic solution. It was concluded that after this treatment, the PLA/graphene filament resistance was reduced by three folds [81].

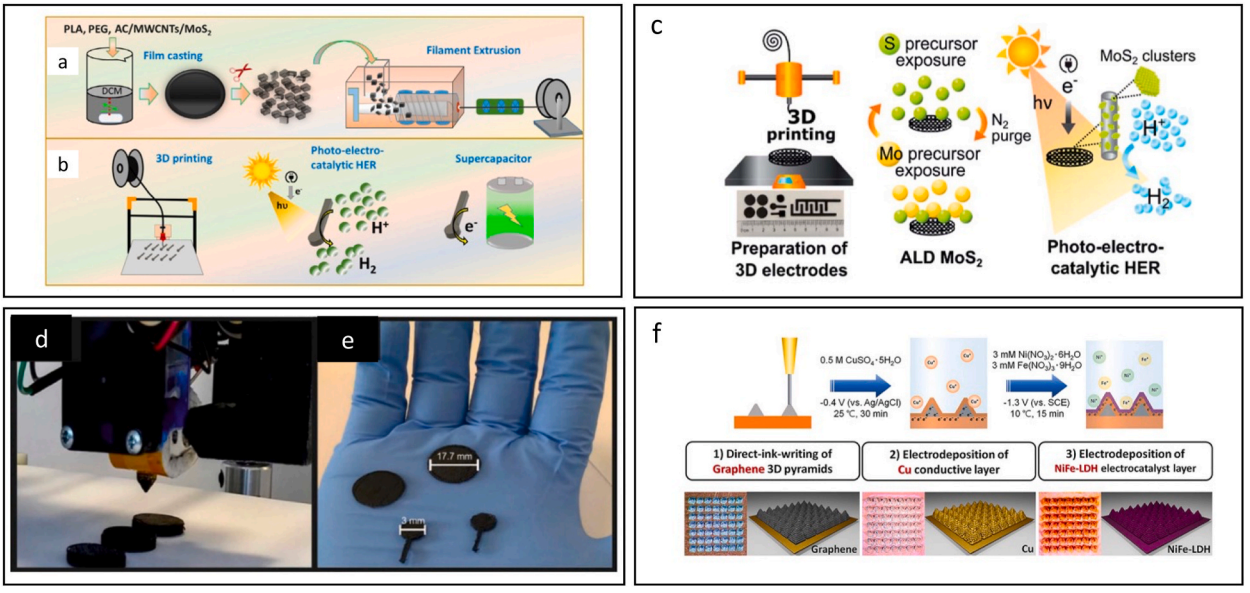

Fig. 7. (a) Schematic flow for the PLA/carbon/MoS_2 filament fabrication and (b) 3D-printing process of PLA/carbon/MoS_2 electrode via FDM techniques and its applications adapted with permission from Ref. [82]. Copyright 2021 Elsevier; (c) Schematic flow for fabricating 3D-printed PLA/nanocarbon electrode with MoS_2 deposited via ALD technique. Adapted with permission from Ref. [83]. Copyright 2021 The Royal Society of Chemistry; (d) 3D-printing of PLA/graphene disk electrode via FDM techniques and (e) Various 3D-printed PLA/graphene electrode structures adapted from Ref. [84] licensed under CC-BY; (f) Schematic representation for the fabrication of 3D-printed electrode derived from ethyl cellulose and graphene in pyramidal arrays deposited with NiFe-LDH. Adapted from Ref. [85]. Licensed under CC-BY.

Table 3
Summary of 3D-printed bio-based polymers used in electrochemical and photoelectrochemical energy conversion.

Bio-based Polymer	Additives	3D Printing Technique	3D Printed Component	Application	Performance	Significance	Ref.
PLA	Cu_2O/modified with sintered Al_2O_3	FDM	Circular shape for photoelectrode	Oxygen evolution reaction	Photocurrent (Iph) = 9.7 A/W	The FDM technique was opted to achieve mass production of the photoelectrode	[88]
PLA	Nickel (Ni) and Platinum (Pt) coated on 3D printed PLA/graphene electrode	FDM	Electrode with no structure specification	Hydrogen evolution reaction	Current density = 10 mA cm^{-2}. Overpotential = 268.7 mV (at 10 mA cm^{-2})	The 3D printing is used to tune the surface area.	[89]
PLA	Ni and copper (Cu) coated on 3D printed PLA/graphene electrode	FDM	Rod-shaped cathode	Hydrogen evolution reaction	Current density = 40.12 mA cm^{-2}	The 3D printing is used to tune the surface area	[53]
PLA	Carbon black	FDM	Rod-shaped with rough layered surface structure for cathode	Preliminary to CO_2 and N_2 reduction to hydrocarbon compound	n/a	The PLA/carbon black was chosen as cost-efficient conductive material. The 3D printing techniquewas used to tune the electride length and introduce surface texture to increase surface area.	[90]
PLA	Graphene (chemically activated using DMF and electrochemically activated using $[Fe(CN)_6]^{3-/4-}$	FDM	Ring-shaped electrodes	Hydrogen evolution reaction	HER activity improved up to ca. 600 mV at current density of −1.5 mA cm^{-2}	The PLA/graphene filament was opted due to its cost-efficiency compared to Pt-based electrodes. The 3D printing was used as rapid fabrication techniques.	[59]
Nylon	Cu/Ni electrodeposited	SLS	Rectangle shape with surface modification of cones, pyramids, cylindric rods, and elliptic (oval) cylinders shape for cathode	Hydrogen evolution reaction	Overpotential = ~250 mV (at 10 mA cm^{-2})	The 3D printing was used to alter electrode topography resulting in better contact to electrolyte and better release of produced H_2 gas.	[57]
	NiFe coated	SLS	Rectangle electrode with porosity for anode	Oxygen evolution reaction	Overpotential = ~300 mV (at 10 mA cm^{-2})	The 3D printing was used to tune the porosity for better mass transfer.	
PLA	Graphene and carbon nanofiber activated in KOH using cyclic voltammetry method	FDM	Rectangular with grid infill pattern for electrode	Hydrogen evolution reaction	Current density = 0.325 (PLA/graphene) and 0.329 mA cm^{-2} (PLA/CNF)	The 3D printing was used to control the uniform dispersion and ratio of the deposited structure.	[91]
PLA	Graphene	FDM	Disk shape for electrode	Hydrogen evolution reaction	Overpotential = −0.46 vs SCE towards HER upon 1000th cycle	The 3D printing enables structural tuning which led to the increment of oxygenated species on the surface of 3D-printed electrode	[84]

(*continued on next page*)

Table 3 (*continued*)

Bio-based Polymer	Additives	3D Printing Technique	3D Printed Component	Application	Performance	Significance	Ref.
PLA	Graphene (with inherent Ti and Fe impurities)	FDM	Rectangular frame for electrode	Photoelectrochemical water oxidation	Current density = 0.46 $mAcm^{-2}$; Overpotential = . −0.85 V vs RHE at −10 mA cm^{-2}.	The PLA/graphene filament was opted due to its cost-efficiency compared to Pt-based electrodes. The 3D printing was used to tune the electrode morphology. DMF and thermal treatment was used to increase the HER performance	[80]
PLA	MoS_2	FDM	Disk shape for electrode	Hydrogen evolution reaction	Current density = 85.7 mA g^{-1}; Overpotential = −450 mV vs RHE at −10 mA cm^{-2}.	The 3D printing was used to tune the incorporation of MoS_2.	[82]
Ethyl Cellulose	Cu_2O/Cu	DIW	Pyramid arrays photocathode	Photoelectrochemical hydrogen evolution reaction	3.01 mA at 0.02 V (vs. RHE)	The 3D printing was used to control the pyramidal arrays structure on the surface of the photoelectrode. The 3D-printed pyramidal arrays directly affect the photon absorption and result in the increment of photocurrent density.	[86]
Ethyl cellulose	Ni-Fe layered double hydroxide	DIW	Pyramid arrays photoanode	Oxygen evolution reaction	Current density = 0.818 μA cm^{-2}; Overpotential = 258 mV at 10 mA cm^{-2}.	The 3D printing was used to alter the surface of electrode into having pyramidal arrays. The fabrication of pyramidal arrays meant to increase the electroactive surface area for the reaction.	[85]
Hydrxypropylmethyl celllulose	MoS_2	DIW	Rectangular lattice with grid infill pattern aerogel for electrode	Hydrogen evolution reaction	Current = 100 mA; Overpotential = ∼ −0.4 V vs RHE at 10 mA cm^{-2}.	The 3D printing was used to tune the surface area of the aerogel.	[87]
Lignin	Graphitic carbon nitride (g-C_3N_4)	DIW	Pillar arrays for photoelectrode	Photoelectrochemical hydrogen evolution reaction	Hydrogen yield = 4.36 μmol (cm^{-2} h^{-1}) at a bias of −0.5 V versus RHE,	The 3D printing was used to fabricate apillar arrays, inspired by wood structure. The pillar arrays were used to modify the g-C_3N_4 into vertically aligned 2D photocatalyst, hence increasing its photon absorption.	[92]

The use of 3D-printed PLA-based electrodes combined with photocatalysts for photoelectrochemical energy conversion is further

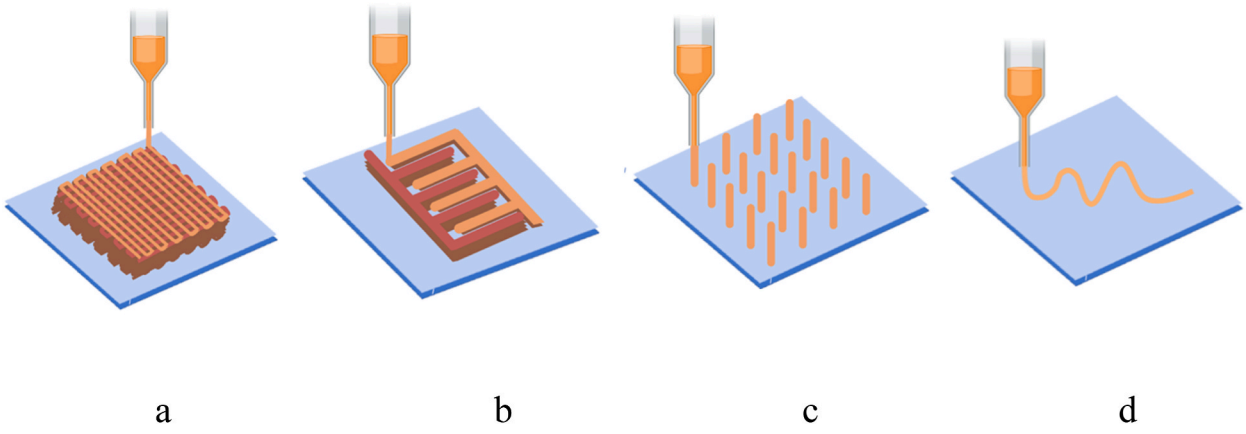

Fig. 8. The (a) woodpile, (b) interdigitated, (c) pillars and (d) fibers designs that are commonly used for 3D-printed energy batteries.

studied. A PLA/Molybdenum disulfide (MoS_2) composite was 3D-printed via the FDM method to obtain photoelectrode for hydrogen production through HER as visualized on Fig. 7a,b. A carbonaceous compound such as activated charcoal (AC) and multiwalled carbon nanotubes (MWCNT) was used as conductive fillers. It was found that the carbon filler and MoS_2 could be loaded up to 80% yet still resulted in a well-defined printing structure. It was concluded that the 3D-printed electrode had significant activity under the visible light region for hydrogen production with 550 mV vs RHE at -10 mA cm^{-2} overpotential value and current density in optimized conditions up to 85.7 mA g^{-1} [82]. Atomic layer deposition (ALD) was also used to introduce MoS_2 as a photocatalyst in the 3D-printed PLA/nanocarbon electrode based on the scheme shown at Fig. 7c. MoS_2 that possessed high electrocatalytic activity toward HER and high photon absorption ability in visible light region was coated onto the printed scaffold using ALD in low temperature with cycle variation between 38 and 900 ALD cycles. This method resulted in crystalline MoS_2 nanoclusters with low sulfur content. The electrode was reported having low overpotential value of 480 mV [83]. PLA/graphene filament known to have HER activity was used to print 3D disk electrodes as an alternative to Platinum (Pt)-based electrodes (Fig. 7d,e). The 3D printed electrode without post printing treatment such as curing process or metal oxides deposition has shown great catalytic performance of -0.46 vs SCE towards HER upon 1000th cycle which was comparable to Pt having the value of -0.25 vs SCE. This high activity was correlated to the use of 3D printing that enables structural tuning which led to the increment of oxygenated species upon the surface of 3D-printed electrode. The use of 3D printing technique has also made possible the fabrication of free-standing electrode with high catalytic activity. It also showed potential for up-scaled fabrication to produce large number of the electrode without the need of post-printing process [84].

Other than PLA, the use of cellulose as a bio-based polymer is recently being explored. Ethyl cellulose-graphene ink was 3D-printed via DIW technique to obtain electrode scaffold. Copper (Cu) and Cuprous Oxide (Cu_2O) then were deposited onto the surface of printed scaffold to induce the photo-electrocatalytic activity. Cu acted as a current collector while the Cu_2O acted as photocatalyst. It was reported that the use of 3D printing technique was used to tune the light absorption area (A_a) which was directly related to the catalytic activity. In this regard, the increment of A_a contributed to the increment of activation sites for carrier generation [86]. The ethyl cellulose/graphene-based ink was used to fabricate a 3D-printed electrode with NiFe-layered double hydroxide (LDH) as depicted on Fig. 7f. The 3D-printed pyramidal arrays coated with the Cu conductive layer and NiFe-LDH photocatalyst has possessed great overpotential value of 314 mV at 10 mA cm^{-1} and exchange current density of 0.818 μA/cm^2. It also exhibited excellent durability as it showed no potential decay for 60 h. This work indicated that cellulose has a great potential to be used for the fabrication of highly active, stable, and low-cost photoelectrode for either HER or OER based on the photocatalyst employed in the system [85]. Another recently published work has employed hydroxypropyl methylcellulose (HPMC)/Pluronic F-127/graphene-based ink to fabricate 3D printed aerogel as an electrode for water splitting. A commercial MoS_2 powder was used as a catalyst and incorporated to the viscous composite ink. Pluronic F-127 blended with HPMC was used as the polymer matrix in the ink formulation as it has profound shear thinning properties. The 3D printed electrode was reported to have electrochemically active surface area up to >1700 cm^2 and were able to produce current up to 100 mA in acidic media. The 3D structure created via DIW printing process has promoted better mass transport within the material thus increasing HER efficiency [87]. Other applications of the 3D-printed bio-based polymer in electrochemical and photoelectrochemical energy conversion are summarized in Table 3.

4. 3D printing of bio-based polymers in energy storage system

High-performing energy storage devices that able to save and port energy promptly with minimum dissipation are essentials following energy generation. Batteries and supercapacitors have been the core technologies for centuries. Since Alessandro Volta's first invention in 1800, batteries have served their purpose as energy storage based on a redox mechanism. During its advancement following the trends in portable electronics, batteries have evolved into high-density with excellent mobility energy storage systems by imposing lithium, sodium, and zinc chemistries [93,94]. Conversely, supercapacitors that work based on electrochemical mechanisms have also undergone monumental development. Through 3 primary mechanisms of electric double-layer capacitance (EDLC),

pseudo-capacitance, and hybrid capacitance, this device has been able to provide higher energy density and a longer life cycle compared to batteries [95]. Although it seems well-established, researchers are continuously looking for the next-generation material for both systems with regard to safety improvement, charge-discharge efficiency, and applicability in advanced components possessing customized properties such as flexibility [96,97]. Herein, the discussion on the fabrication of customized and highly efficient batteries and supercapacitor employing 3D-printed bio-based polymers will be covered.

4.1. Batteries

As the main technology powering human daily life, batteries have continuously evolved to meet the current needs of energy storage. 3D printing has unlocked the possibility for the battery system to have more design and structural freedom, improving the overall storage mechanism and its applicability in a customized device. Typically, traditional batteries are made through a process that

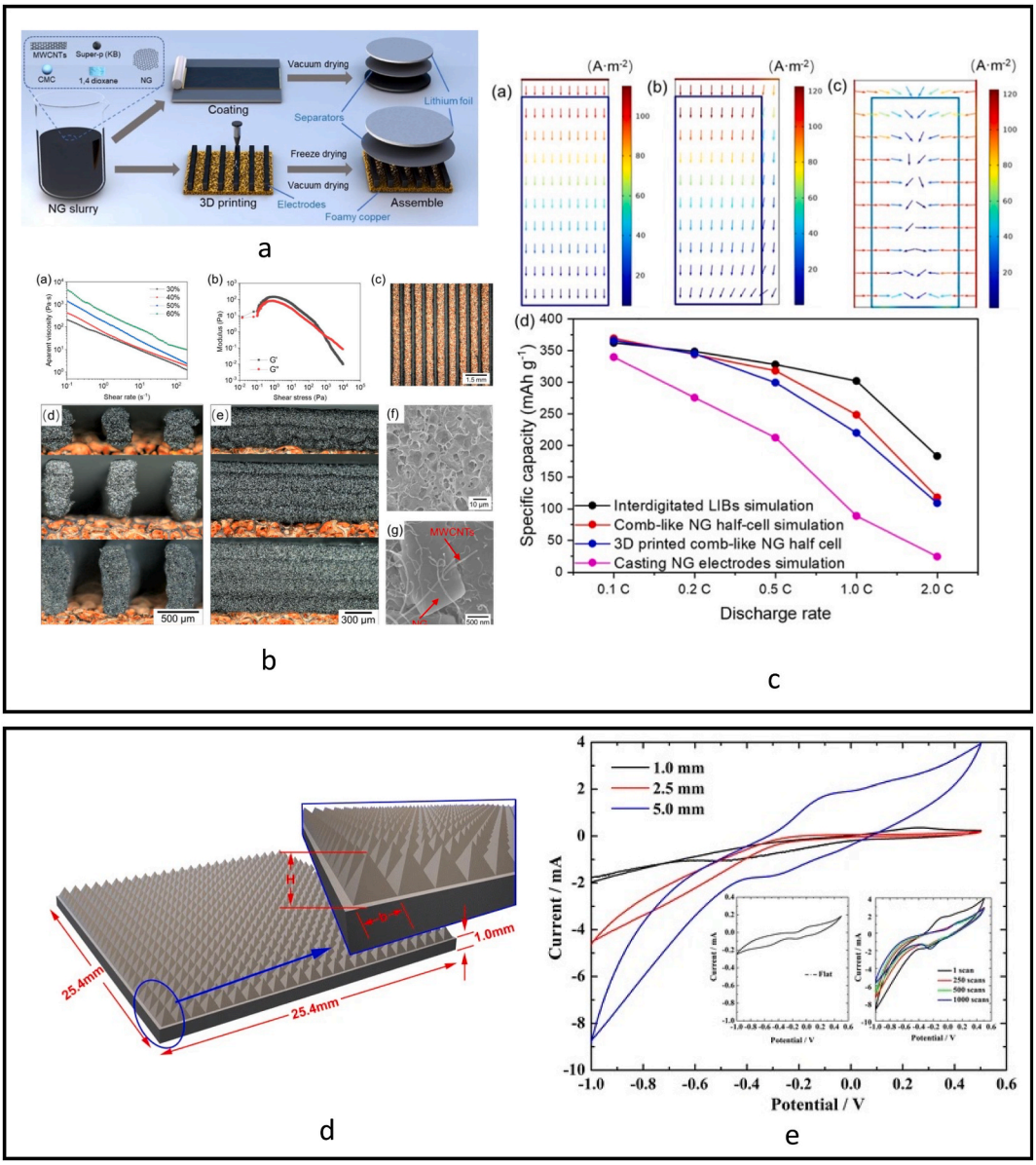

Fig. 9. (a) Schematic visualization of the 3D comb-like electrode; (b) apparent viscosity and rheological behavior of the 3D printing ink, top and intersectional view of the 3D comb-like electrode, and SEM imaging of the electrode; (c) Simulation Li-ions transport and the capacity fade comparison between the 3D-printed comb-like electrode with the casted electrodes adapted with permission from Ref. [107] copyright of Elsevier 2022; (d) 3D printed pyramidal arrays of PLA/graphene and (e) the cyclic voltammogram of the 3D printed electrode with a variation on the pyramid height as compared to flat-printed structure adapted with permission from Ref. [108]. Copyright of Springer Nature, 2017.

involves creating mixtures of electrode slurry, which are then cast onto current collectors. The cell components are then stacked together and packed into metal canisters or pouch films. Finally, the liquid electrolyte was injected into the battery [98]. However, this process makes structural modification or size reduction difficult, which was later found achievable via 3D printing [99]. Employing 3D printing techniques to fabricate a unique structure in battery assemblies also allows a higher mass percentage of incorporated active materials. It increases the surface-to-volume ratio thus reducing the distance for ion transport that leads to elevated total power density [100]. In term of geometrical design, the commonly used printed structures for batteries are depicted in Fig. 8. The woodpile structure (Fig. 8a) consists of alternating layers that are stacked perpendicularly to each other, inducing the formation of macro-sized pores that could promote electrolyte and ion diffusion. This structural configuration is highly stable and provides a high surface area [50]. The interdigitated structure as depicted in Fig. 8b consists of interdigitated side-by-side finger-like shape that is favorable due to the small distance between electrodes thus promoting shorter length for ion diffusion pathways. It is also beneficial due to the possibility of

Table 4
Summary of 3D-printed bio-based polymers used in batteries.

Bio-based Polymers	Additives in Ink Formulation	3D Printing Technique	Electrolyte	Structure	Significance	Ref.
CMC	$LiFePO_4$ and PEDOT:PSS	DIW	$LiPF_6$	Woodpile thick electrode.	The 3D printing was used to control the electode technique. CMC was used to facilitate high loading of the active material. Maximum area capacitance was 5.63 mAh cm^{-2}, 0.2C with 92% capacity retention over 100 cycle at 1.43 mm electrode thickness.	[112]
CMC	$LiCoO_2$, surfactant, carbon black	Inkjet Printing	$LiPF_6$	Thick planar electrode	The 3D printing allow the customized thickness of the electrode. The discharge current density was 180 μA cm^{-2}. The initial discharge capacity was 120 mAh/g, and the capacity loss of 5% after 100 cycles.	[113]
CMC	LFP powder, Triton X, carbon	Drop on Demand	$LiPF_6$	Accidented cathode	The 3D printing was used to lower the distance between electrodes. The specific capacity was 140 at 1C rates.	[114]
CNF	Multiwalled carbon nanotube (MWCNT)	DIW	Li_2S	3D porous scaffold	The 3D printing was used to fabricate internal porosity to facilitate Li-ion transport. The areal capacity was 5 mA h cm^{-2} for 50 cycles and withstand ≥500 cycles	[115]
PLA	$LiFePO_4$	FDM	$LiPF_6$ and LiTFSI–PYR_{14}TFSI ionic-liquid electrolyte	disc, spiral and double-spiral LFP cathode and LTO anode	The 3D printed spiral structure helped to reduce continuous volume change during charge-discharge cycle. The voltage profile of the LFP-PLA cathode cycled between 3.8 and 2.6 V is presented as a function of capacity at 9 μA cm^{-2}, 44 μA cm^{-2} and 88 μA cm^{-2} charge- and discharge-current densities. The cycling of the cell resulted in 60, 50 and 20 mA h g^{-1} for LFP at 9, 44 and 88 μA cm^{-2}. While, specific capacity of the Li/LTO cell is 80 mA h g^{-1}	[116]
Hemicellulose and starch	Eutectic gallium-indium liquid metal alloy, polyacrylamide, and carbon black.	DIW	$ZnSO_4$	Grid anode	Current density of 0.5 mA cm^{-2} after 50 charge-discharge cycles. The composite exhibited a long lifetime of over 700 h (up to 1500 cycles) with a low voltage hysteresis (178 mV at a current density of 1.44 mA cm^{-2})	[117]
PLA	Activated carbon, poly (acrylic acid) (PAA), and polyaniline (PANI)	FDM	$ZnSO_4$	3D Carbon framework cathode	PAA and PANI was used to tailor the crystallinity of PLA to result in conductive PLA-based substrate. (3D@PANI-PAA) presents a reversible capacity of 214.6 mAh g^{-1} at 0.4 A g^{-1}, rate performance of 117.2 mAh g^{-1} at 3.2 A g^{-1}, and cycling stability over 1000 cycles with 78.1% capacity retention.	[118]

fabricating an assembly without separator [84,101]. The pillar arrays (Fig. 8c) are commonly used for vertical aligning of 1D or 2D active material. This structure is mainly highlighted for its high surface area and ability to facilitate better interfacial contact between electrode active materials with liquid electrolyte. However, 3D pillar structure may require particular rheological properties to obtain geometrical stability [102]. Meanwhile, the fiber structure (Fig. 8d) is widely used for wearable devices as it is favored for its flexibility [103]. This freedom of design in battery fabrication could lead to the increment of area energy density, area power density, and volumetric energy density [26].

On the other side, recent advances have shown the current favorability of the use of bio-based polymers in the 3D-printed battery assembly. This class of polymer is taking the role of enabling the printability of active materials such as metal oxides, carbonaceous compounds, or ionic salts in electrolytes. The use of bio-based polymeric materials as binding agents allows a higher amount of loaded active material in the composite when compared to commonly used rheological modifiers or binding agents such as CNT, graphene, or poly(vinylidene fluoride) (PVDF). Excellent printability despite the presence of inorganic material is made possible by the dispersion ability and rheological properties of bio-based polymers [104,105]. All these merits provided by the bio-based polymers are at lower cost than other materials, thus elevating the sustainability value of the overall manufacturing process [106].

A 3D comb-like electrode based on natural graphite was printed with the aid of carboxymethyl cellulose (CMC) resulting printed line width of 260 μm indicating excellent fidelity of the printed structure. The 3D comb-like structure was proven to have reduced capacity fade (365.8 mAh g^{-1} @ 0.1C to 108.7 mAh g^{-1} @ 2.0C) compared to the traditionally tape-casted electrode which had drastic capacity fade (339.4 mAh g^{-1} @ 2.0C to 24.1 mAh g^{-1} @ 2.0C). It was caused by the rapid Li-ions transport in the 3D-printed comb-like architecture caused by its possibility to move laterally between cathodes and anodes as depicted on Fig. 9a–c [107]. A unique 3D pyramidal array was also successfully fabricated via FDM printing using PLA as a binder for graphene, as visualized in Fig. 9d,e. It was found that the highest printed pyramid (5 mm) results in high specific discharge capacity (65 mAh g^{-1} with retention of 93% after 1000 cycles). The higher the pyramid size also promoted higher amount of graphene loading. It was also reported that this unique structure was beneficial for the charge transfer in the electrode interface thus increasing Li^{+} intercalation performance [108]. PLA/graphene was employed to fabricate a porous anode to be a part of Lithium-ion (Li-ion) battery. The fabrication of printing filament allows the precise variation of graphene loaded in the battery architecture. The effect of graphene on the conductivity was investigated, and the result showed that 20 wt% of graphene content yielded efficient conductivity. The NaOH treatment prior to the printing process induced a porous structure which resulted in the specific capacity of 500 mAh g^{-1} at a 40 mAh g^{-1} current density value [7].The comparison of 3D printing and conventional roller coating method in order to control solid loading and electrode thickness in the $LiFePO_4$ (LFP) cathode was reported. The high solid content of 0.467 g mL^{-1} with a thickness of 115 μm resulted in the best rate capacities of 82 mAh g^{-1} @ 10C. In contrast, control over electrode thickness is impossible to be obtained using roller coating [109]. The advantage of 3D printing to fabricate micro-batteries was also demonstrated. CNF was used to aid the printing process of the LFP electrode. The shear thinning behavior and porosity affected by CNF addition have led to the improvement of printability, ion accessibility and inducing lowered local current density. The printed CNF-$LiFePO_4$ cathode exhibited 80 mAh g^{-1} at a 10 °C charge-discharge rate with capacity retention of 85% over 3000 cycles [110].

Flexible and wearable batteries for use in portable electronics are also possible to be fabricated via 3D printing techniques. A 3D serpentine pattern derived from CNF and CNT was 3D printed using the DIW technique. It was found that the use of CNC not only induces the printability for LFP batteries but also enhances the mechanical properties due to its high aspect ratio and strong interaction with CNT. The electrode showed excellent stretchability and had a reversible capacitance of 353 mAh g^{-1} at the 100th charge-discharge cycle after 50% stretched for 50 times [104]. A 3D-printed wearable electronic in the form of a bangle having an integrated battery was fabricated using PLA via FDM techniques. This study reported the modification of PLA filament using ethyl methyl carbonate, propylene carbonate, and LiClO4 to induce ionic conductivity in the material. The assembled coin cell had energy and power densities of 0.14 Wh L−1 and 0.83 W L−1. It was able to power green LED light for approximately 36s [111]. Other applications of 3D-printed bio-based polymers in battery components are summarized in Table 4.

4.2. Supercapacitor

Supercapacitors are energy storage devices that employ a reversible process of adsorption and desorption of ions in the electrolytes-electrodes interface, enabling the storage and discharge of chemical energy. Based on their mechanism, supercapacitors are divided into three types: EDLC, pseudo capacitor, and hybrid capacitor. The common EDLC assembly comprises two electrodes, a separating membrane, and an electrolyte. EDLC stores energy by adsorbing ions drawn on the electrode's surface when the electricity is applied. Meanwhile, the energy-storing mechanism of the pseudo capacitor is based on continuous reversible redox reactions between the electrode-electrolyte system. Lastly, the hybrid capacitor works based on the combination of the aforementioned mechanisms, faradaically and nonfaradaically [95,119]. Traditionally, supercapacitors are known to be fabricated using screen printing, template-assisted structuring, and holographic lithography which is vulnerable in terms of constructing precisely customized structures. Other than that, those methods are complicated, time-consuming, and often include using toxic chemicals to remove the templates [120].

The 3D printing techniques have been employed in the fabrication of supercapacitors owing to their ability to control thickness and morphology to elevate ion conductivity. Additionally, bio-based polymer is chosen as a binder or viscosity enhancer in the 3D printing ink formulation mainly to replace the use of current binders that are toxic and possessed poor mechanical properties [121]. The use of bio-based polymers is also favorable to minimize the environmental footprint as it enables possible degradation at the end of its life cycle. It was due to the presence of various chemical functionalities within the bio-based polymer backbone that is susceptible to degradation [105]. A recent report presented the fabrication of electro-conducting aerogels derived from CNF and CNT which was

highlighted for their capacitive performance and recyclability. 3D printing was used to tune the surface area and also enabled the large-scale production of the aerogel. The as-prepared aerogel possessed a conductivity of 30.95 S cm^{-1} with a capacitance of 551 F g^{-1} after the incorporation of MnO_2. The composite aerogel was solidified through freeze-thawing followed by a freeze-drying process; thus, any means of chemical crosslinking was not present. Therefore, through this fabrication strategy, a degradable aerogel was achieved [122]. Another disposable, nontoxic, and high-performing EDLC supercapacitor based on nanocellulose was reported. Nanocellulose such as CNF and CNC were used as rheological modifiers. The swelling of nanocellulose upon contacting with the electrolyte was proven to enhance the accessibility of ion diffusion into the printed electrode. The capacitance of the 3D-printed EDLC was 25.6 F g^{-1} with an operating voltage of up to 1.2 V. According to the report, the 3D-printed electrode derived from the aforementioned material could be degraded by 50% within a period of 9 weeks [123].

Recent report has been made on the use of cellulose for the fabrication of supercapacitor schematically represented in Fig. 10a–e. Cellulose nanofiber (CNF) procured from oil palm fiber via alkaline treatment, oxidation using 2,2,6,6-tetramethylpiperidine-1-oxyl (TEMPO), and ultrasonification was used as an additive to adjust the rheological properties of $Ti_3C_2T_x$ MXene-based ink. $Ti_3C_2T_x$ which is a negatively charged 2D transition metal carbides, nitrides and carbonitride, has been known for its potent redox activity and good conductivity. In spite of its good properties, there were difficulties to use standalone $Ti_3C_2T_x$ for 3D printing process due to its unsuitable viscoelastic behavior at low concentration. In this regard, CNF was used to elevate $Ti_3C_2T_x$ viscoelastic properties (Fig. 10f–n). The optimum condition followed by post-printing treatment using freeze drying method has enabled the fabrication of interdigitated, self-standing and hierarchically porous scaffold which had improved surface area, ion transport ability and superior capacitive performance. The solid interdigitated printed scaffold was reported having 2.02 F cm^{-2} areal capacitance, 101 μWh cm^{-2} energy density and 0.299 mW cm^{-2} power density, while maintaining capacitance retention rate of 85% over 5000 cycles (Fig. 10o–t). The similar system was prepared using FDM techniques employing PLA/graphene. It was reported that the presence of impurities such

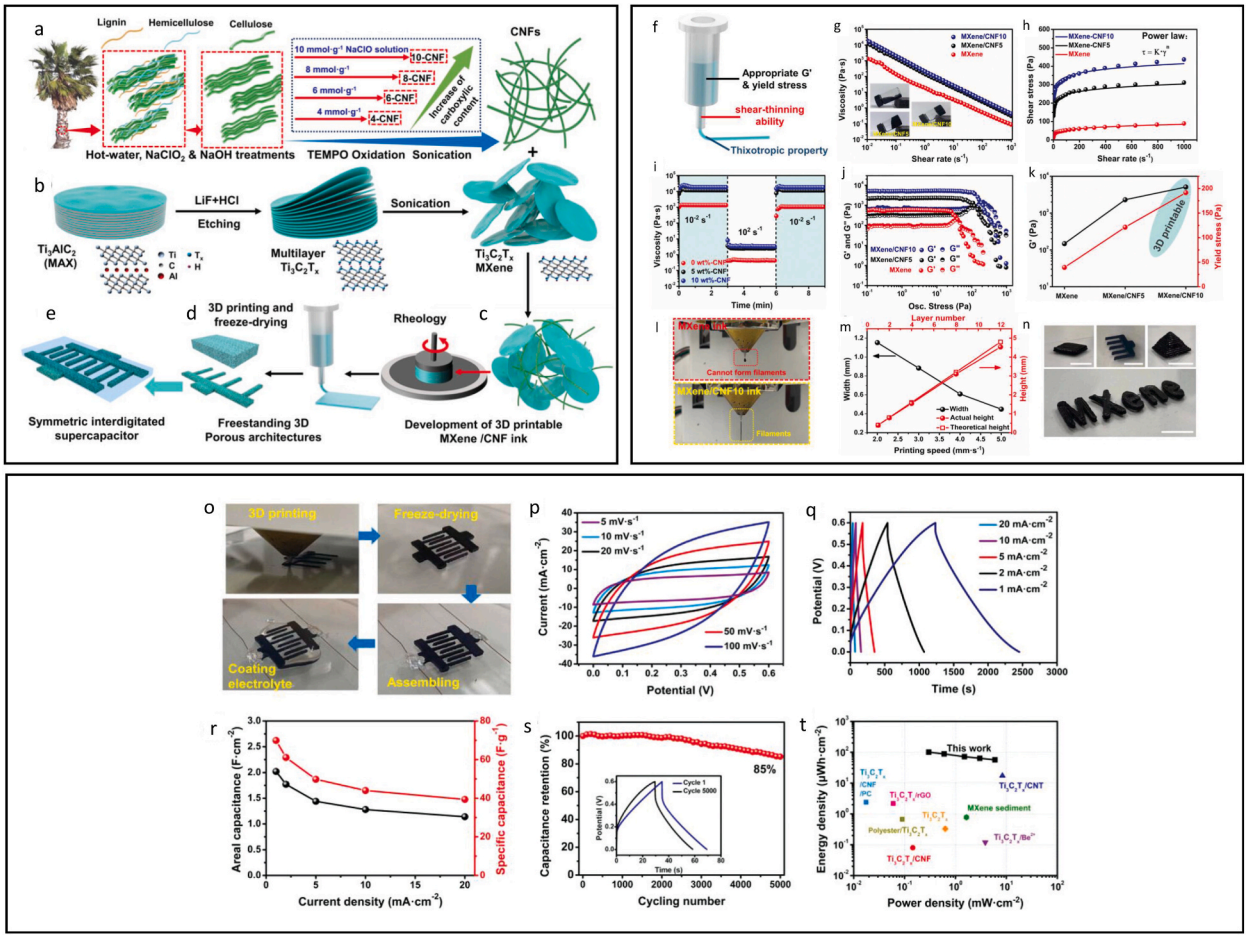

Fig. 10. (a)–(e) schematic flow of the 3D printed $Ti_3C_2T_x$.CNF based electrode; (f) required rheological properties for the 3D-printed $Ti_3C_2T_x$, (g) viscosity change vs shear rate, (h) Shear stress vs shear rate and its fitting to the power law, (i) viscosity evolution over time, (j) G' and G'' function of oscillatory stress, (k) G' at plateau regions and yield stress point, (l) the image of printed filament, (m) the width of printed filament in relation with printing speed, (n) image of printed scaffold; (o) image of printed electrode during fabrication process, (p) cyclic voltammetry (CV) profile at 5–100 mV S^{-1} scan rate, (q) GCD profiles from 1 to 20 mA cm^{-2}, (r) area and specific capacitance, (s) cycling performance, (t) Ragone plots of comparison between electrode fabricated in this work with others. Adapted with permission from Ref. [124]. Copyright 2021 Wiley-VCH GmbH.

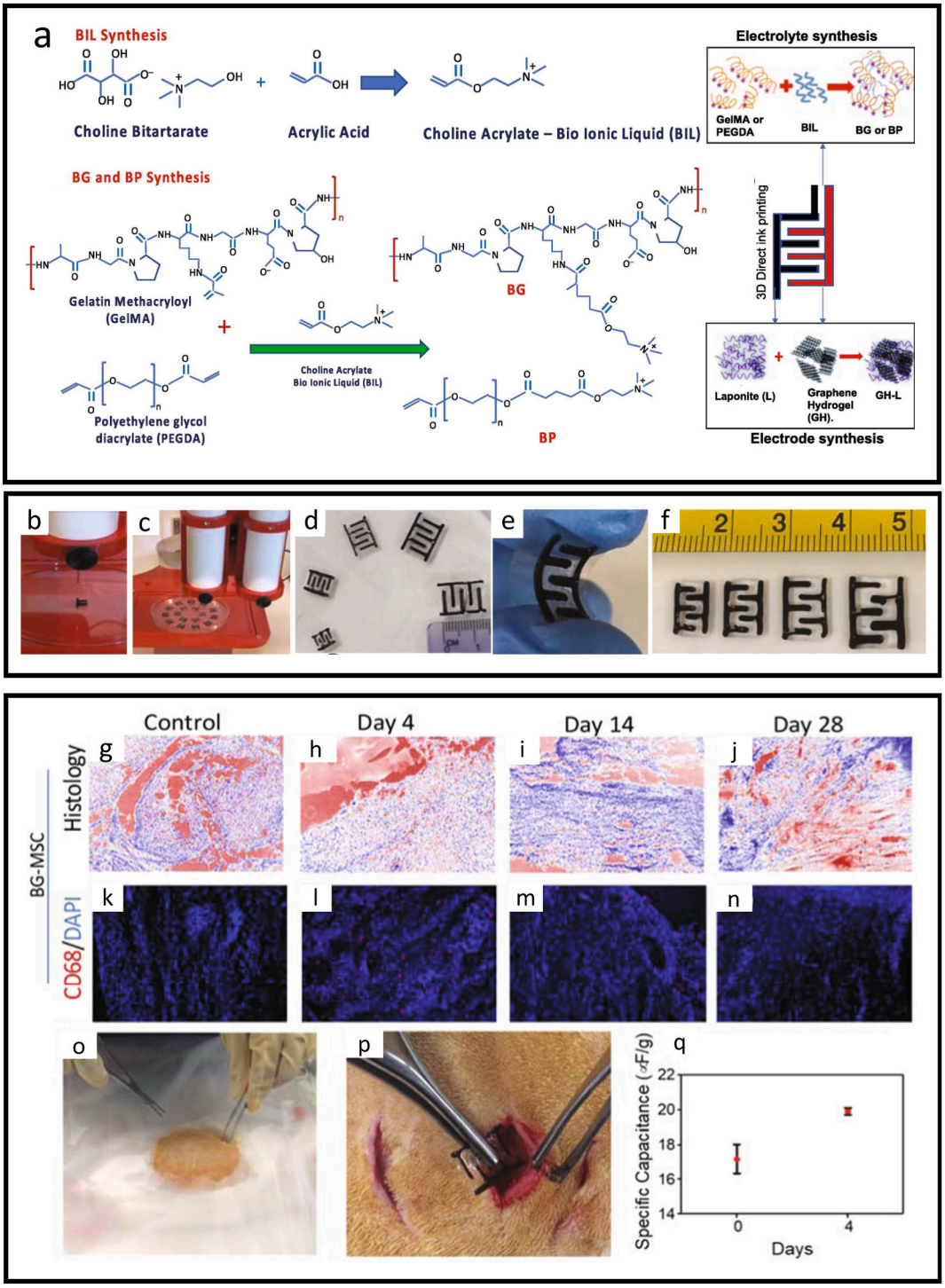

Fig. 11. (a) Synthesis and fabrication pathways of gelatin and choline-derived biocompatible micro-supercapacitor.; (b–c) 3D printing process of the gelatin-derived bio-electrolyte along with the electrode in the micro-supercapacitor assembly while (d–f) is the visual image of 3D-printed electrode in various size.; *In vivo* biocompatibility and degradation assay, (g–j) Hematoxylin and Eosin (H&E) staining of the printed device and surrounding tissue in the variation of implantation period, (k–n) fluorescent immunohistochemical analysis with D68 macrophage presence in various implantation period, (o–p) subcutaneous implantation of the micro-supercapacitor, and (q) the retention of specific capacitance value during implantation. Adapted with permission from Ref. [126]. Copyright of Elsevier 2021.

Table 5
Summary of 3D-printed bio-based polymers used in supercapacitor.

Bio-based Polymers	Additives in Ink formulation	3D Printing Technique	Structure	Capacitance	Significance	Ref.
CNF	Single-walled carbon nanotube (SWCNT) and urea.	DIW	Woodpile structure	11.8 F cm^{-2}	The 3D printed structure allows the fabrication of thick (12.2 mm) and high-loaded (85.1 mg cm^{-2}) capacitor. The device provided flash charging within 3.6 s.	[132]
CNF	CNT and MnO_2	DIW		551 F g^{-1}	The 3D printable CNF/CNT composite aerogel was obtained through freeze-thawing and ambient-drying process. The composite was recyclable due to the absence of chemical crosslinking within the matrix.	[133]
Gelatin	Polyethylene glycol diacrylate (PEGDA), choline, Lithium phenyl-2,4,6-trimethylbenzoylphosphinate (LAP)	DIW	Gel elctrolyte between interdigitated electrodes	200F g^{-1}	3D printing was used to fabricate interdigitated micro supercapacitor. Gelatin was used as a biocompatible material.	[126]
CNC	SiO_2	DIW	Electrode in woodpile architecture	148.6 F g^{-1}	3D printing of CNC and SiO_2 with freeze drying as post-printing treatment created micro-, meso-, and macroporous structure beneficial for ion diffusion through the capacitor.	[134]
CNF	$Ti_3C_2T_x$	DIW	Interdigitated electrode	2.02 F cm^{-2}	CNF was used as an ink rheological modifier for the fabrication of solid-state supercapacitor with interdigitated structure. CNF was used instead of highly concentrated MXenes pure ink to prevent self restacking upon drying. The composite resulted in real capacitance of 2.02 F cm^{-2}, energy density of 101 μWh cm^{-2} at a power density of 0.299 mW cm^{-2}, with a capacitance retention rate of 85% after 5000 cycles.	[124]
Alginate	Alginate, Cellulose, PEDOT:TOS	DIW	Rectangular supercapacitor with honeycomb infill	78 F g^{-1}	The alginate-CNF was used to fabricate 3D-printed aerogel that potentially loaded with poly(3,4-ethylenedioxythiophene): tosylate (PEDOT:TOS) by *in situ* polymerization.	[55]
PLA	Graphene and TiO_2 and Fe_3O_4 impurities	FDM	Disk electrode	135 mF cm^{-2}	The effect of TiO_2 impurities in commercial PLA/graphene filament was investigated. Electrode was 3D printed to tune the surface area and thermally carbonized as a post-printing modification strategy, resulted in a high capacitive material.	[135]
CMC	Kapok-derived carbon tile, SWCNT, $NiCo_2O_4$	DIW	Electrode in cubic lattice structure	588 mF cm^{-2}	CMC was used as dispersant to facilitate ultrahigh loading of the active material and 3D printability. The excellent performances of 588 mF cm^{-2} specific capacitance, 138 μWh cm^{-2}, and stability for 88% over 5000 cycles were reported owing to the fabrication of unimpeded channels for ion diffusion via 3D printing.	[136]
CNC	SiO_2	DIW	Cubic lattice	148.6 F.g–1	CNC was used to fabricate 3D structure with high fidelity. The printed porous structure was beneficial to facilitate electrolyte diffusion in the supercapacitor system.	[54]
Alginate	$Ti_3C_2T_x$	DIW	Curve patterned structure	2.7 F cm^{-2}	Alginate was chosen as bio-based polymer that could be crosslinked by Ca^{2+}. The interlayer interaction of alginate aided by Ca^{2+} promoted better electron transport in the supercapacitor system. The 3D curvy pattern was chosen to promote flexibility in the supercapacitor.	[52]
CMC	Graphene	DIW	Cubic lattice	2265.19 mF. cm^{-2}	The 3D printing was used to tune surface area by varying the printing layer	[137]

(*continued on next page*)

Table 5 (*continued*)

Bio-based Polymers	Additives in Ink formulation	3D Printing Technique	Structure	Capacitance	Significance	Ref.
					height. CMC was chosen for its superior rheological properties to facilitate high loading of the graphene.	
CNC	–	SLA	Ring shaped	43.4 pF	The CNC was modified using methacrylic acid to make it photocurable.	[138]

as Ti and Fe in the ion or oxide form attached onto the PLA/graphene filament could reduce the capacitance value. After removal of the impurity, the 3D printed electrode possessed 135 mF cm^{-2} capacitance at current density of 0.92 mA cm^{-2}. It also been reported that the cyclic stability for 100% capacitance retention was found up to 2000 cycles [124].

The non-toxicity of bio-based polymers also enables the fabrication of biocompatible 3D- printed supercapacitors with potential use in bioelectronic devices. The potential of gelatin for fabricating 3D-printed hydrogel having capacitive performance was also recently reported. Gelatin functionalized with methacrylate end group was blended with acrylate-functionalized choline bio-ionic liquid resulting in an electrically conductive hydrogel. The 3D DIW-printed hydrogels were reported to have an electronic conductivity value of 27×10^{-2} S/cm. The gelatin-choline hydrogel demonstrated impressive compatibility with cells and effectively adhered to the skin, indicating its potential as a versatile substance for constructing bioelectronic devices [125]. Another report presented the use of gelatin as a 3D-printed polymer electrolyte in a micro-supercapacitor to refrain from using conventional electrolyte compounds which potential leakage could induce toxic responses in the human body. The methacrylated gelatin blended with acrylated choline serves as a bio-ink with sufficient rheological properties to be subjected directly to DIW printing with preparation scheme presented in Fig. 11a. The polymer electrolyte was positioned between two interdigitated electrodes based on 3D-printed graphene in a complete assembly of flexible and implantable micro-supercapacitor (Fig. 11b–f). Biocompatibility of the 3D-printed supercapacitor was presented by the viability of 91% of C2C12 cells seeded in the electrolyte surface. The immunogenicity, *in vivo* degradation, and capacity retention were also investigated by implanting the 3D-printed micro-supercapacitor via subcutaneous implantation in an animal. The result showed that the devices were able to retain their specific capacitance within 4 days (Fig. 11q), underwent enzymatic biodegradation within 28 days, and showed excellent biocompatibility with no toxic response to the surrounding tissues at 28-day post-implantation (Fig. 11g–p) [126].

Another avenue for utilizing 3D printing techniques in fabricating supercapacitors is device miniaturization. A 3D-printed miniaturized supercapacitor comes with the significance of excellent areal capacitance, outstanding rate capability, rapid charge-discharge, and longer life cycle despite its compact size as a result of efficient ionic species migration in the electrochemical system that are achievable through structural modification and optimization of active material composition, which is difficult to be obtained using traditional fabrication methods such as casting and screen printing. A milli- to micro-ranged size of the miniaturized supercapacitors is also beneficial for certain applications such as wearable electronics, bioelectronics, and sensors [127,128]. The fabrication of a micro supercapacitor with a good areal capacitance of 30.00 mF cm^{-2} is achievable via 3D printing of ethyl cellulose, graphene, and carbon sphere composite. Ethyl cellulose was employed not only as a rheological modifier and dispersing agent for carbonaceous compounds but also as a porogen that was eliminated through thermal annealing. The variety in pores profile in the 3D printed structure was proven to elevate its areal energy density [129].

The fabrication of multicomponent in supercapacitors assembly was also done using 3D printing. It was reported that a multimaterial 3D printing technique was done to fabricate outer packaging and the current collector of a supercapacitor. A custom-made 3D printer construction was made to accommodate the FDM nozzle employing PLA filament to print the supercapacitor frame and paste extruder employing CMC as a rheological modifier to deposit the current collector, electrode layer, and separator. Through a careful computerized command tailored as a g-code, an orchestrated fabrication using a combined FDM-DIW technique allows for a time-, cost-, and material-efficient process to fabricate fully printed supercapacitors. The EDLC supercapacitor fabricated using this strategy was reported to have a specific capacitance of 193.20 mF g^{-1} [120]. A core-sheath structure of a pseudo capacitor employing molybdenum disulfide (MoS_2) as the active material along with graphene and CNT as a current collector was printed at once using a co-axial two capillary printhead. CMC was chosen to facilitate the printability and dispersibility of the active material both in the core and outer shell. Due to excellently intact core-shell configurations, the electrolyte diffusion into the core pseudocapacitive material was enhanced, boosting the charge transport within the material. It was reported that this material possessed a specific capacitance of 558 mF cm^{-2}, energy density of 49 μWh cm^{-2}, and stability of 87% over 8000 cycles [130]. An electronic textile based on patterned cloth using 3D printing was fabricated using CNT and silk fibroin-based ink. CNT and silk fibroin ink were extruded in a core-sheath structure using a 3D printer equipped with a co-axial nozzle. The printed fiber patterned on fabric material was investigated for its capacitance resulting in 26.42 mF cm^{-2} at a current density of 0.42 mA cm^2 owing to good charge transport between the fiber electrodes. It also presented good flexibility and mechanical stability under a series of deformations, indicating its potential for developing smart textile material [131]. Other applications of 3D printing using bio-based materials for the fabrication of supercapacitors and their unique characteristics are summarized in Table 5.

5. Cost analysis

To initiate a comprehensive cost analysis for fabricating energy devices using both conventional and 3D printing methods employing bio-based polymers, a systematical examination of various cost components associated with raw materials, equipment, labor, and energy consumption, was elaborated to derive a detailed and informative understanding of the economic considerations involved in each manufacturing approach. The fabrication of commercially available Li-ion battery with well-known manufacturing process as the targeted product was adapted [139]. As cost values are very dependent on geographical consideration the price point on every incurred expenses is based on the United States (US) standard in this description. This analysis is solely intended to provide an overview for comparison regarding cost profiling related to the use of 3D printing in the fabrication process and bio-based polymers as an alternative battery material compared to conventional methods.

An overview of the stepwise manufacturing process model for Li-ion batteries both using conventional and 3D-printing processes, is depicted in Fig. 12. In this model, LFP, LTO, $LiPF_6$, Super P, and PP are chosen as model cathode, anode, electrolyte, conducting and separator disk material, respectively. Traditional production methods involve blending all active materials with PVDF as a binder into a slurry, which is subsequently fed into a coating machine for deposition onto current collectors. Following the drying phase, the resulting sheet undergoes calendering to regulate thickness and density (Fig. 12a). The assembled cathode, anode, and separator are then cut out into the desired shape and subjected to electrolyte injection (Fig. 12b). Ultimately, the assembly is packaged to obtain the final Li-ion battery product (Fig. 12c). Meanwhile, the fabrication of Li-ion batteries via 3D printing begins with pre-printing

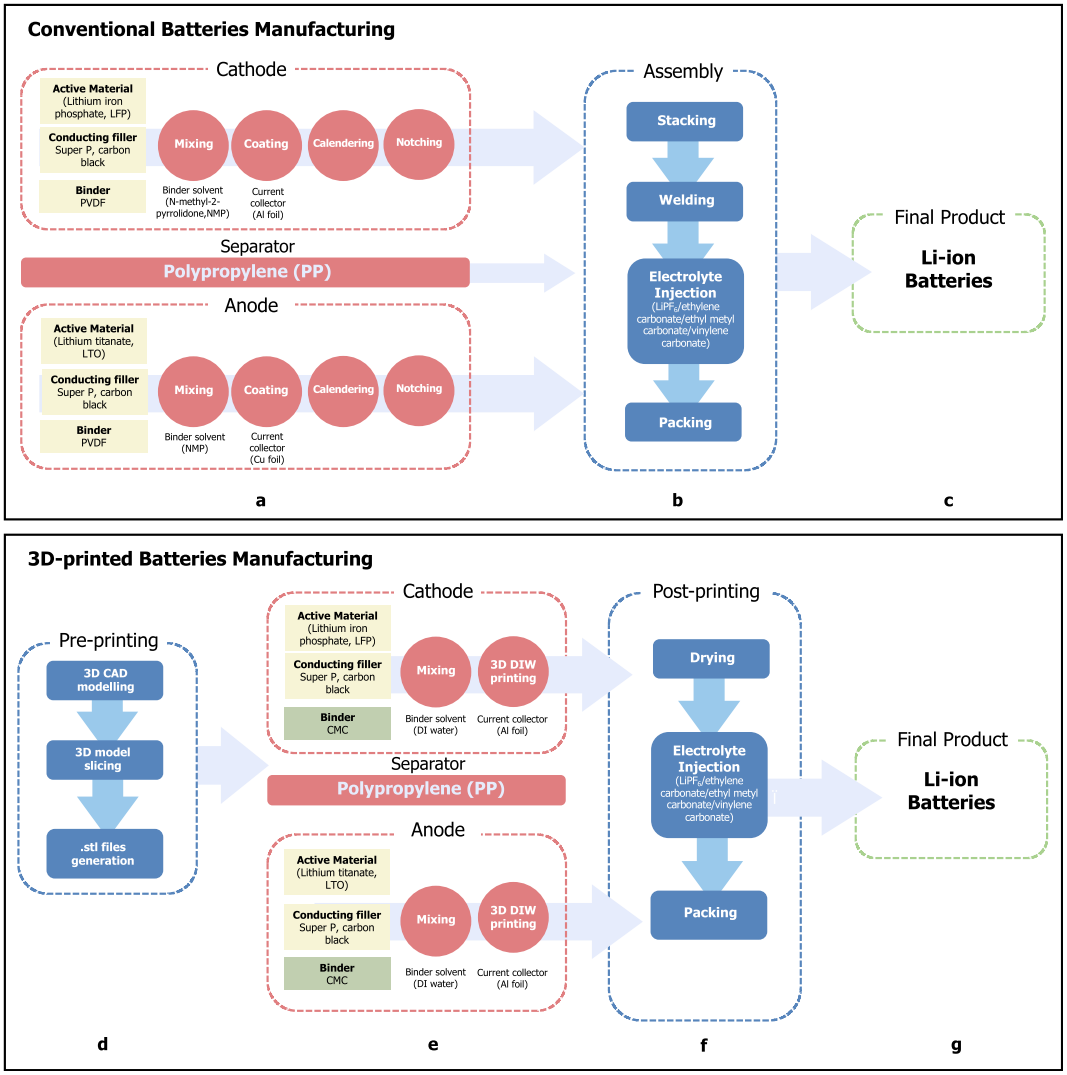

Fig. 12. Li-ion battery manufacturing process via conventional method including (a) anode, cathode, and separator fabrication, (b) battery cell assembly, and (c) final conventional battery product processes; and 3D-printing technique using bio-based polymer as material feedstock including (d) pre-printing, (e) 3D printing of anode, cathode, and separator, (f) post-printing treatment, and (g) final 3D-printed batteries product.

preparation, as depicted in Fig. 12d. The 3D model was designed as per the desired final product geometry and functionalities. The designed model was then digitally sliced layer-per-layer and converted into *.stl* file format to be processable in a 3D printer. The 3D printing ink was formulated by dispersing all the active material in DI water and adding CMC as a binder and rheological modifier. The ink formulation is printed using an extrusion-based DIW technique based on the designed 3D models (Fig. 12e). As 3D printing offers freedom in geometrical modification, thickness and density could be regulated during this process without additional equipment. After printing, the 3D structure is sequentially subjected to drying, electrolyte injection, and packing to obtain the final 3D-printed Li-ion battery product (Fig. 12f–g).

The cost component for projected expenses in each manufacturing step is presented in Table 6 and Fig. 13a,d. Based on raw material costs, substituting PVDF as a common binder in battery manufacturing with a bio-based binder such as CMC could reduce the production cost (Fig. 13b,e). As most bio-based materials do not require the use of organic solvent, the cost could be further minimized. The equipment ownership cost of each conventional battery manufacturing production line and 3D DIW printing as the most suitable technique in battery manufacturing have been presented. In small-scale production, it could be seen that the cost of a conventional battery production line is similar to a single 3D DIW printer (Fig. 13c,f). This presented that employing 3D printing in battery manufacturing is still economically challenging. Nevertheless, the advantages of utilizing 3D printing cannot be overlooked due to its ability to offer geometric freedom, which is directly linked to the improvement of volumetric, areal energy, and areal power density [26]. Targeted manufacturing by using 3D printing could as well reduce the waste production compared to the conventional material manufacturing, which from cost perspectives will also reduce the cost incurred by post-production waste management process [140]. The minimum energy use by 3D printing-based manufacturing (Table 6) compared to the conventional process also could aid to reduce the production cost. In general, the use of bio-based material and 3D printing techniques in battery manufacturing could lower overall production cost. Thus, emphasizes the economic feasibility of adopting 3D printing of bio-based material for the production of energy devices.

Table 6
Cost modelling for Li-ion battery fabrication via conventional and 3D printing employing bio-based polymer method.

No	Cost Component	Cost (USD)	Quantity	Unit	Required unit		Total cost unit (USD)	
					Conventional Method	3D-printing	Conventional Method	3D-printing
Raw Material								
A. Electrode material								
1	LTO[a]	1300	1	kg	1	1	1300	1300
2	LFP[a]	1400	1	kg	1	1	1400	1400
3	Al foil[a]	1	1	m	1	1	1	1
4	Cu foil[c]	3	1	m	1	1	3	3
5	Super P, carbon black[c]	1000	1	kg	1	1	1000	1000
B. Binder Material								
11	PVDF[a]	2000	1	kg	1	1	2000	
12	CMC[a]	250	1	kg		1	0	
13	NMP[a]	600	1	L	1	–	600	
14	DI Water[a]	30	1	L	–	1		
B. Electrolyte Material								
5	$LiPF_6$[b]	1600	1	kg	1	1	1600	1600
6	Ethylene carbonate[a]	100	1	kg	1	1	100	100
7	Ethyl methyl carbonate[a]	4000	1	L	1	1	4000	4000
8	Vinylene carbonate[a]	3200	1	kg	1	1	3200	3200
C. Separator								
10	PP[a]	250	1	kg	1	1	250	250
Equipment								
15	TMAX laboratory vacuum homogenizer for battery slurry	1080	1	Unit	1	1	1080	1080
16	TMAX electric lab calendar roller for Li-ion Battery	2000	1	Unit	1	–	2000	0
17	TMAX ultrasonic Metal Welder	4380	1	Unit	1	–	4380	0
18	STYLER battery spot welder	1300	1	Unit	1	–	1300	0
19	Recon Biotech Tissuebot 3D DIW Printer	7500	1	Unit	–	1	0	7500
Labor								
20	Labor worker[d]	190	1	day	1	1	190	190
Energy								
21	Electricity (Estimated 6 operating hours/day)	0.16	1	kWh	23[e]	2[e]	3.68	0.32
Grand Total							24,008	21,505

[a] Cost quoted from Sigma-Aldrich, USA.
[b] Cost quoted from TCI Chemicals, India.
[c] Cost quoted from Nanografi, USA.
[d] Wages based on standard salary range presented in the USA region by GlassDoor.
[e] Calculated based on the total power (W) needed for each machine in the manufacturing line.

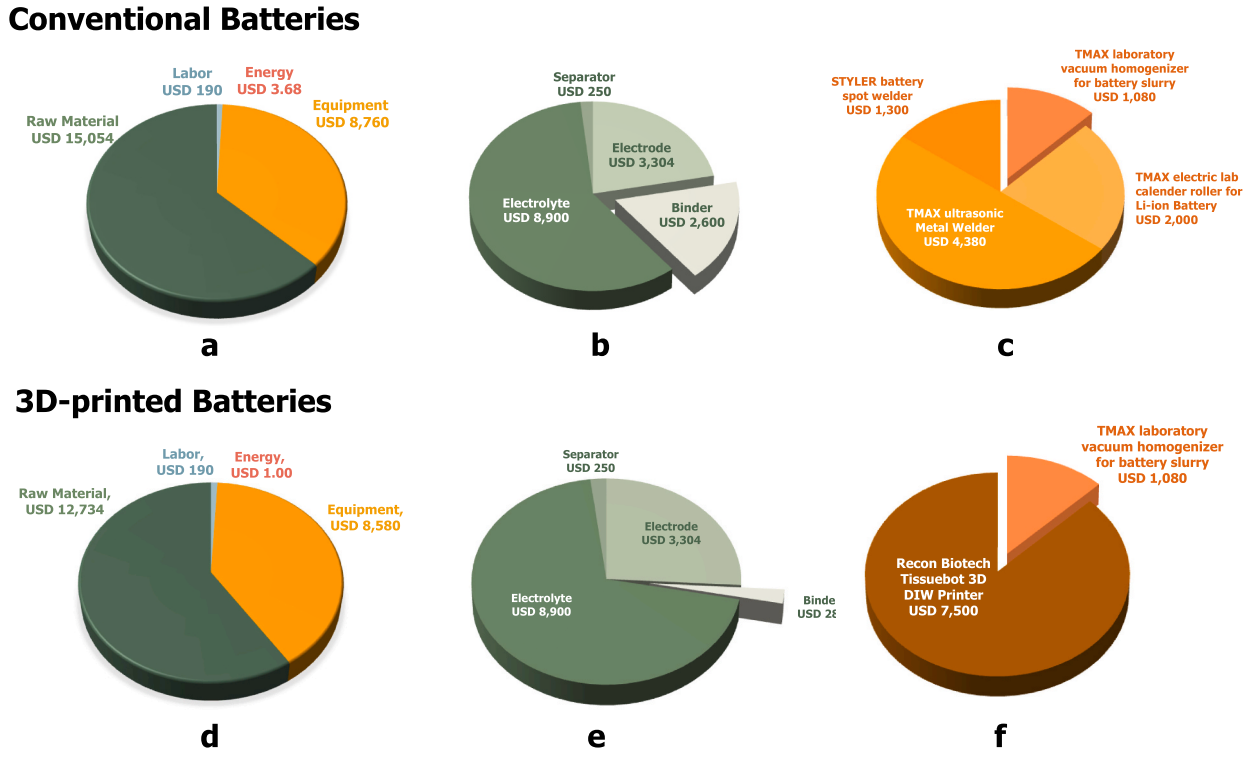

Fig. 13. Cost component comparison in battery manufacturing via conventional (a) and 3D-printing integrating bio-based polymer (d) in term of raw material (b,e) and equipment (c,f).

6. Conclusions and future perspective

The current significance of the emerging trends of 3D-printed bio-based polymer material to fabricate key components in energy conversion and storage systems has been thoroughly reviewed. The fabrication via 3D printing has enabled geometrical freedom to obtain beneficial structures for each component application. The geometrical freedom spans from the fabrication of thick electrodes with a maximum loading capacity of active material to the fabrication of micro-components to be utilized in mobile and implantable devices. Various patterns ranging from the porous lattice, serpentine, interdigitated to vertical arrays to facilitate better mass, ion, and photon transport in energy conversion and storage systems were also successfully achieved via 3D printing and proven to elevate the conversion and storage performance.

Furthermore, employing bio-based polymers as a base of ink material in 3D printing has allowed the possibility to obtain high structural fidelity of the printed geometries owing to their inherent physical and rheological properties. Through presented cost analysis, their incorporation could reduce total production cost. It also possessed lower toxicity when compared to conventional material used in the fabrication of energy devices such as metals, synthetic polymer (i.e. PVDF), and inorganic viscosity enhancer (i.e. graphene). Hence, the 3D-printed bio-based polymer brought new avenues to the fabrication of bio-compatible energy components, thus extending the application into advanced technologies such as *in vivo* implantable energy storage devices, wearable bioelectronics, and components for energy conversion employing microorganisms such as MFCs. Other than that, the use of bio-based polymer has introduced better degradability at the end-of-life cycle of the energy components making it more environmentally friendly.

The aforementioned merits of featuring 3D-printed bio-based material in energy conversion give valuable insights that this fabrication strategy may serve as efforts to achieve sustainability in energy storage and conversion systems. The use of 3D printing techniques well-known for their rapid manufacturing and ability to control the generated waste due to thoroughly calculated material deposition contributes on the responsible consumption and production goal based on UN's SDGs. Moreover, bio-based polymers that are mostly nature-derived employed in the process will lower the production of carbon footprint hence may serve as an act to prevent climate change. The improvement of overall energy conversion and storage after the implementation of 3D-printed and bio-based polymers as reviewed suggests that this strategy may serve as a way to obtain more sustainable clean energy sources for all.

Through this review, it is known that extrusion-based 3D printing particularly the most suitable technique to fabricate energy devices, considering the necessity of incorporating heterogenous active materials. However, solely depending on this technique is still challenging in term of performance and economic perspective. In energy device fabrication, the future outlook will be full control over microporosity to aid with the mass transport of bulk material. Meanwhile, 3D printing could provide ease of control over material bulk porosities; this ability is very dependent on the nozzle dimension in extrusion-based equipment. Although currently the 3D micro- to nanoprinting has been made possible, it suffers from the commercial availability of the nozzle and compatibility of the ink [141,142].

Other than that, from economic perspective, the total technology cost of using extrusion-based 3D printing is considerably high. FDM-based printers are commercially available at a low cost. However, additional filament-making processes prior to 3D printing require additional equipment and cost. Ideally, 3D integral printing using DIW printers are favored due to the ease of processing, but the total cost for equipment ownership is still relatively high as presented in Section 5. Therefore, future development on the low-cost 3D DIW-based printers and commercially available high-resolution nozzle is crucial to facilitate the scalability and better control of desired energy devices morphology. The development of compatible ink with good dispersion of highly loaded active materials should also become a concern to enable the 3D printing of high-resolution energy devices.

Alternatively, future outlook on the use of other printing technique such as SLA should be well considered. SLA printing technique is widely known for its superior ability to fabricate intricate structure including 3D structure having hierarchical porosity as compared to extrusion-based techniques. This printing technique also makes possible the fabrication of multi object at once, hence reducing the production time [143]. Due to the high demand for this technology, SLA-based printers are widely available in relatively low prices. Additionally, employing bio-based material using SLA technique is possible. Several bio-based polymers such as gelatin [144,145], chitosan [146], and silk [146] modified with the photopolymerizable group could be printed into complex structures via the SLA printing technique. Preserving the core principles of energy device manufacturing with a focus on sustainability and high efficiency.

The attempt to integrate bio-based polymers into 3D-printed energy device fabrication is also still in the state of infancy, especially in the material processing aspect. Numerous bio-based polymers remain unexplored. Chitin and chitosan, for instance, rank as the second most abundant bio-based materials in nature, but their utilization in 3D-printed energy devices remains limited. They exhibit excellent 3D printability. The nitrogen group in its polymer backbone has been reported to act as an excellent electrochemical substrate for energy devices. The N atom acts as dopant that could link to the improvement of the carbon substrate conductivity, contributing to charge transfer within energy devices [19,147,148]. Other than that, S atom contained in keratin could also serve the same purpose [79]. Therefore, the exploration towards other kind of bio-based polymers with diverse functional groups may be an interesting direction for the development of 3D-printed energy devices.

Data availability

No data was used for the research in the article.

CRediT authorship contribution statement

Khoiria Nur Atika Putri: Writing – original draft, Conceptualization. **Varol Intasanta:** Writing – review & editing. **Voravee P. Hoven:** Writing – review & editing, Supervision, Funding acquisition.

Declaration of competing interest

The authors declare that they have no known competing financial interests or personal relationships that could have appeared to influence the work reported in this paper.

Acknowledgements

The authors would like to extend our gratitude to Chulalongkorn University for the support of review writing. We are also grateful to Chulalongkorn University and the National Science and Technology Development Agency (NSTDA) for granting a doctoral fellowship to Ms. Khoiria Nur Atika Putri under the Chulalongkorn University-NSTDA Scholarship program.

References

[1] Z. Wang, Y. Wang, Z. Wang, Q. He, C. Li, S. Cai, 3D printing of electrically responsive PVC gel actuators, ACS Appl. Mater. Interfaces 13 (2021) 24164–24172, https://doi.org/10.1021/acsami.1c05082.
[2] S. Deepak Kumar, G. Arun Manohar, R. Surya Teja, The state of art 3D printing: a case study of Ganesh Idol, Mater. Today Proc. 56 (2022) 455–461, https://doi.org/10.1016/j.matpr.2022.01.418.
[3] N. Li, K. Tong, L. Yang, X. Du, Review of 3D printing in photocatalytic substrates and catalysts, Mater. Today Energy 29 (2022) 101100, https://doi.org/10.1016/j.mtener.2022.101100.
[4] A. Tanwilaisiri, R. Zhang, Y. Xu, D. Harrison, J. Fyson, A manufacturing process for an energy storage device using 3D printing, in: Proc. IEEE Int. Conf. Ind. Technol., 2016, pp. 888–891, https://doi.org/10.1109/ICIT.2016.7474869, 2016-May.
[5] J.L. Sanchez Noriega, N.A. Chartrand, J.C. Valdoz, C.G. Cribbs, D.A. Jacobs, D. Poulson, M.S. Viglione, A.T. Woolley, P.M. Van Ry, K.A. Christensen, G. P. Nordin, Spatially and optically tailored 3D printing for highly miniaturized and integrated microfluidics, Nat. Commun. 12 (2021), https://doi.org/10.1038/s41467-021-25788-w.
[6] I.F. Mena, M.A. Montiel, C. Sáez, M.A. Rodrigo, Improving performance of proton-exchange membrane (PEM) electro-ozonizers using 3D printing, Chem. Eng. J. 464 (2023), https://doi.org/10.1016/j.cej.2023.142688, 0–7.
[7] C.W. Foster, G.Q. Zou, Y. Jiang, M.P. Down, C.M. Liauw, A. Garcia-Miranda Ferrari, X. Ji, G.C. Smith, P.J. Kelly, C.E. Banks, Next-generation additive manufacturing: tailorable graphene/polylactic(acid) filaments allow the fabrication of 3D printable porous anodes for utilisation within lithium-ion batteries, Batter. Supercaps. 2 (2019) 448–453, https://doi.org/10.1002/batt.201800148.
[8] L. Chen, X. Tang, P. Xie, J. Xu, Z. Chen, Z. Cai, P. He, H. Zhou, D. Zhang, T. Fan, 3D printing of artificial leaf with tunable hierarchical porosity for CO_2 photoreduction, Chem. Mater. 30 (2018) 799–806, https://doi.org/10.1021/acs.chemmater.7b04313.
[9] C.Y. Lee, A.C. Taylor, S. Beirne, G.G. Wallace, 3D-Printed conical arrays of TiO_2 electrodes for enhanced photoelectrochemical water splitting, Adv. Energy Mater. 7 (2017) 1–6, https://doi.org/10.1002/aenm.201701060.

[10] C.Y. Lee, A.C. Taylor, A. Nattestad, S. Beirne, G.G. Wallace, 3D printing for electrocatalytic applications, Joule 3 (2019) 1835–1849, https://doi.org/10.1016/j.joule.2019.06.010.

[11] M.A. Abdelkareem, K. Elsaid, T. Wilberforce, M. Kamil, E.T. Sayed, A. Olabi, Environmental aspects of fuel cells: a review, Sci. Total Environ. 752 (2021) 141803, https://doi.org/10.1016/j.scitotenv.2020.141803.

[12] M.K. Khawaja, A. Alkhalidi, S. Mansour, Environmental impacts of energy storage waste and regional legislation to curtail their effects – highlighting the status in Jordan, J. Energy Storage 26 (2019) 100919, https://doi.org/10.1016/j.est.2019.100919.

[13] H. Li, Y. Li, S. Zhu, Y. Li, I. Zada, Y. Li, Recent advances in biopolymers-based carbon materials for supercapacitors, RSC Adv. 13 (2023) 33318–33335, https://doi.org/10.1039/d3ra06179e.

[14] E.G. Bahçegül, E. Bahçegül, N. Özkan, 3D printing of hemicellulosic biopolymers extracted from lignocellulosic agricultural wastes, ACS Appl. Polym. Mater. 2 (2020) 2622–2632, https://doi.org/10.1021/acsapm.0c00256.

[15] J. Liu, L. Sun, W. Xu, Q. Wang, S. Yu, J. Sun, Current advances and future perspectives of 3D printing natural-derived biopolymers, Carbohydr. Polym. 207 (2019) 297–316, https://doi.org/10.1016/j.carbpol.2018.11.077.

[16] N. Li, D. Qiao, S. Zhao, Q. Lin, B. Zhang, F. Xie, 3D printing to innovate biopolymer materials for demanding applications: a review, Mater. Today Chem. 20 (2021), https://doi.org/10.1016/j.mtchem.2021.100459.

[17] S. Keshipour, M. Hadidi, O. Gholipour, J. Ling, A review on hydrogen generation by photo-, electro-, and photoelectro-catalysts based on chitosan, chitin, cellulose, and carbon materials obtained from these biopolymers, Adv. Polym. Technol. 2023 (2023), https://doi.org/10.1155/2023/8835940.

[18] R. Singh, H.W. Rhee, The rise of bio-inspired energy devices, Energy Storage Mater. 23 (2019) 390–408, https://doi.org/10.1016/j.ensm.2019.04.030.

[19] A.S.M. Wittmar, M. Ropertz, M. Braun, U. Hagemann, C. Andronescu, M. Ulbricht, Preparation of N-doped carbon materials from cellulose:chitosan blends and their potential application in electrocatalytic oxygen reduction, Polym. Bull. 80 (2023) 7827–7845, https://doi.org/10.1007/s00289-022-04429-2.

[20] G. Gopinath, S. Ayyasamy, P. Shanmugaraj, R. Swaminathan, K. Subbiah, S. Kandasamy, Effects of biopolymers in energy storage applications: a state-of-the-art review, J. Energy Storage 70 (2023) 108065, https://doi.org/10.1016/j.est.2023.108065.

[21] M. Shahbazi, H. Jäger, Current status in the utilization of biobased polymers for 3D printing process: a systematic review of the materials, processes, and challenges, ACS Appl. Bio Mater. 4 (2021) 325–369, https://doi.org/10.1021/acsabm.0c01379.

[22] H. Kodama, Automatic method for fabricating a three-dimensional plastic model with photo-hardening polymer, Rev. Sci. Instrum. 52 (1981) 1770–1773, https://doi.org/10.1063/1.1136492.

[23] J.S. Jayan, B.D.S. Deeraj, A. Saritha, K. Joseph, Biopolymer-derived carbonaceous composites and their potential applications, in: Hybrid Nat. Fiber Compos. Mater. Formul. Process. Charact. Prop. Eng. Appl., Elsevier Ltd., 2021, pp. 253–280, https://doi.org/10.1016/B978-0-12-819900-8.00005-2.

[24] M.P. Browne, E. Redondo, M. Pumera, 3D printing for electrochemical energy applications, Chem. Rev. 120 (2020) 2783–2810, https://doi.org/10.1021/acs.chemrev.9b00783.

[25] Y. Jiang, F. Guo, Y. Liu, Z. Xu, C. Gao, Three-dimensional printing of graphene-based materials for energy storage and conversion, SusMat 1 (2021) 304–323, https://doi.org/10.1002/sus2.27.

[26] Z. Lyu, G.J.H. Lim, J.J. Koh, Y. Li, Y. Ma, J. Ding, J. Wang, Z. Hu, J. Wang, W. Chen, Y. Chen, Design and manufacture of 3D-printed batteries, Joule 5 (2021) 89–114, https://doi.org/10.1016/j.joule.2020.11.010.

[27] R. Singh, S. Gautam, B. Sharma, P. Jain, K.D. Chauhan, Biopolymers and their classifications, in: Biopolym. Their Ind. Appl., Elsevier Inc., 2021, pp. 21–44, https://doi.org/10.1016/b978-0-12-819240-5.00002-x.

[28] N. Paxton, W. Smolan, T. Böck, F. Melchels, J. Groll, T. Jungst, Proposal to assess printability of bioinks for extrusion-based bioprinting and evaluation of rheological properties governing bioprintability, Biofabrication 9 (2017), https://doi.org/10.1088/1758-5090/aa8dd8.

[29] X. Duan, J. Xu, Z. Wei, J. Ma, S. Guo, S. Wang, H. Liu, S. Dou, Metal-free carbon materials for CO2 electrochemical reduction, Adv. Mater. 29 (2017) 1–20, https://doi.org/10.1002/adma.201701784.

[30] T. Dalgleish, J.M.G. Williams, A.-M.J. Golden, N. Perkins, L.F. Barrett, P.J. Barnard, C. Au Yeung, V. Murphy, R. Elward, K. Tchanturia, E. Watkins, Polymer Morphology, 2007.

[31] D.H. Chang, Rheology and Processing of Polymeric Materials, Oxford University Press, 2007.

[32] A. Schwab, R. Levato, M. D'Este, S. Piluso, D. Eglin, J. Malda, Printability and shape fidelity of bioinks in 3D bioprinting, Chem. Rev. 120 (2020) 11028–11055, https://doi.org/10.1021/acs.chemrev.0c00084.

[33] D.R. Picout, S.B. Ross-Murphy, Rheology of biopolymer solutions and gels, Sci. World J. 3 (2003) 105–121, https://doi.org/10.1100/tsw.2003.15.

[34] M.A. Hubbe, P. Tayeb, M. Joyce, P. Tyagi, M. Kehoe, K. Dimic-Misic, L. Pal, Rheology of nanocellulose-rich aqueous suspensions: a review, Bioresources 12 (2017) 9556–9661.

[35] T. Ma, L. Lv, C. Ouyang, X. Hu, X. Liao, Y. Song, X. Hu, Rheological behavior and particle alignment of cellulose nanocrystal and its composite hydrogels during 3D printing, Carbohydr. Polym. 253 (2021) 117217, https://doi.org/10.1016/j.carbpol.2020.117217.

[36] V. Kokol, Y.B. Pottathara, M. Mihelčič, L.S. Perše, Rheological properties of gelatine hydrogels affected by flow- and horizontally-induced cooling rates during 3D cryo-printing, Colloids Surf. A Physicochem. Eng. Asp. 616 (2021), https://doi.org/10.1016/j.colsurfa.2021.126356.

[37] H. Li, S. Liu, L. Li, Rheological study on 3D printability of alginate hydrogel and effect of graphene oxide, Int. J. Bioprinting. 2 (2016) 54–66, https://doi.org/10.18063/IJB.2016.02.007.

[38] J. Triyono, H. Sukanto, R.M. Saputra, D.F. Smaradhana, The effect of nozzle hole diameter of 3D printing on porosity and tensile strength parts using polylactic acid material, Open Eng. 10 (2020) 762–768, https://doi.org/10.1515/eng-2020-0083.

[39] P. Czyżewski, D. Marciniak, B. Nowinka, M. Borowiak, M. Bieliński, Influence of extruder's nozzle diameter on the improvement of functional properties of 3D-printed PLA products, Polymers 14 (2022), https://doi.org/10.3390/polym14020356.

[40] A. Brandley, R. Hollfelder, S. Nesaei, B. Vanwie, N. Abu-Lail, B.A. Gozen, Direct-ink-writing of degradable carboxymethylcellulose, Procedia Manuf. 26 (2018) 993–1002, https://doi.org/10.1016/j.promfg.2018.07.130.

[41] V.C.F. Li, C.K. Dunn, Z. Zhang, Y. Deng, H.J. Qi, Direct ink write (DIW) 3D printed cellulose nanocrystal aerogel structures, Sci. Rep. 7 (2017), https://doi.org/10.1038/s41598-017-07771-y.

[42] J. Wang, L.L. Shaw, Rheological and extrusion behavior of dental porcelain slurries for rapid prototyping applications, Mater. Sci. Eng. 397 (2005) 314–321, https://doi.org/10.1016/j.msea.2005.02.045.

[43] Y. He, F. Yang, H. Zhao, Q. Gao, B. Xia, J. Fu, Research on the printability of hydrogels in 3D bioprinting, Sci. Rep. 6 (2016) 1–13, https://doi.org/10.1038/srep29977.

[44] S. Naghieh, X. Chen, Printability–a key issue in extrusion-based bioprinting, J. Pharm. Anal. 11 (2021) 564–579, https://doi.org/10.1016/j.jpha.2021.02.001.

[45] A.H. Pelofsky, Surface tension-viscosity relation for liquids, J. Chem. Eng. Data 11 (1966) 394–397, https://doi.org/10.1021/je60030a031.

[46] K. Fakhruddin, M.S.A. Hamzah, S.I.A. Razak, Effects of extrusion pressure and printing speed of 3D bioprinted construct on the fibroblast cells viability, IOP Conf. Ser. Mater. Sci. Eng. 440 (2018), https://doi.org/10.1088/1757-899X/440/1/012042.

[47] E. Alfredo Campo, Thermal properties of polymeric materials, in: Sel. Polym. Mater., 2008, pp. 103–140, https://doi.org/10.1016/B978-0-8155-1551-7.50005-X.

[48] S.L. Buchwalter, Semiconductor chip underfill materials, in: Encycl. Mater. Sci. Technol., 2001, pp. 8332–8335, https://doi.org/10.1016/b0-08-043152-6/01492-3.

[49] D. A, N. Yodo, A systematic survey of FDM process parameter optimization and their influence on Part Characteristics, J. Manuf. Mater. Process. 13 (2019), https://doi.org/10.1038/s41598-023-28674-1.

[50] C. Reyes, R. Somogyi, S. Niu, M.A. Cruz, F. Yang, M.J. Catenacci, C.P. Rhodes, B.J. Wiley, Three-dimensional printing of a complete lithium ion battery with fused filament fabrication, ACS Appl. Energy Mater. 1 (2018) 5268–5279, https://doi.org/10.1021/acsaem.8b00885.

[51] C.Y. Foo, H.N. Lim, M.A. Mahdi, M.H. Wahid, N.M. Huang, Three-dimensional printed electrode and its novel applications in electronic devices, Sci. Rep. 8 (2018) 1–11, https://doi.org/10.1038/s41598-018-25861-3.

[52] J. Yang, Y. Wang, J. Du, F. Bu, Q. Cao, T. Meng, X. Xu, C. Guan, 3D-printed flexible supercapacitors with multi-level bonded configuration via ion cross-linking, J. Mater. Chem. A 10 (2022) 16409–16419, https://doi.org/10.1039/d2ta04379c.

[53] B. Hüner, N. Demir, M.F. Kaya, Electrodeposition of NiCu bimetal on 3D printed electrodes for hydrogen evolution reactions in alkaline media, Int. J. Hydrogen Energy 47 (2022) 12136–12146, https://doi.org/10.1016/j.ijhydene.2021.10.009.

[54] B. Yao, H. Peng, H. Zhang, J. Kang, C. Zhu, G. Delgado, D. Byrne, S. Faulkner, M. Freyman, X. Lu, M.A. Worsley, J.Q. Lu, Y. Li, Printing Porous Carbon Aerogels for Low Temperature Supercapacitors, 2021, https://doi.org/10.1021/acs.nanolett.0c04780.

[55] H. Françon, Z. Wang, A. Marais, K. Mystek, A. Piper, H. Granberg, A. Malti, P. Gatenholm, P.A. Larsson, L. Wågberg, Ambient-Dried, 3D-printable and electrically conducting cellulose nanofiber aerogels by inclusion of functional polymers, Adv. Funct. Mater. 30 (2020), https://doi.org/10.1002/adfm.201909383.

[56] F. Novotný, V. Urbanová, J. Plutnar, M. Pumera, Preserving fine structure details and dramatically enhancing electron transfer rates in graphene 3D-printed electrodes via thermal annealing: toward nitroaromatic explosives sensing, ACS Appl. Mater. Interfaces 11 (2019) 35371–35375, https://doi.org/10.1021/acsami.9b06683.

[57] R.A. Márquez, K. Kawashima, Y.J. Son, R. Rose, L.A. Smith, N. Miller, O.A. Carrasco Jaim, H. Celio, C.B. Mullins, Tailoring 3D-printed electrodes for enhanced water splitting, ACS Appl. Mater. Interfaces 14 (2022) 42153–42170, https://doi.org/10.1021/acsami.2c12579.

[58] B. Yao, S. Chandrasekaran, J. Zhang, W. Xiao, F. Qian, C. Zhu, E.B. Duoss, C.M. Spadaccini, M.A. Worsley, Y. Li, Efficient 3D printed pseudocapacitive electrodes with ultrahigh MnO 2 loading, Joule 3 (2019) 459–470, https://doi.org/10.1016/j.joule.2018.09.020.

[59] M.P. Browne, F. Novotný, Z. Sofer, M. Pumera, 3D printed graphene electrodes' electrochemical activation, ACS Appl. Mater. Interfaces 10 (2018) 40294–40301, https://doi.org/10.1021/acsami.8b14701.

[60] R. Gusmão, M.P. Browne, Z. Sofer, M. Pumera, The capacitance and electron transfer of 3D-printed graphene electrodes are dramatically influenced by the type of solvent used for pre-treatment, Electrochem. Commun. 102 (2019) 83–88, https://doi.org/10.1016/j.elecom.2019.04.004.

[61] S. Shiva Kumar, V. Himabindu, Hydrogen production by PEM water electrolysis – a review, Mater. Sci. Energy Technol. 2 (2019) 442–454, https://doi.org/10.1016/j.mset.2019.03.002.

[62] M. Ashraf, M. Ayaz, M. Khan, S.F. Adil, W. Farooq, N. Ullah, M. Nawaz Tahir, Recent trends in sustainable solar energy conversion technologies: mechanisms, prospects, and challenges, Energy Fuels (2022), https://doi.org/10.1021/acs.energyfuels.2c04077.

[63] P. Banoth, C. Kandula, P. Kollu, Introduction to electrocatalysts, ACS Symp. Ser. 1432 (2022) 1–37, https://doi.org/10.1021/bk-2022-1432.ch001.

[64] S. Choi, C. Kim, J.M. Suh, H.W. Jang, Reduced graphene oxide-based materials for electrochemical energy conversion reactions, Carbon Energy 1 (2019) 85–108, https://doi.org/10.1002/cey2.13.

[65] S.P.S. Badwal, S.S. Giddey, C. Munnings, A.I. Bhatt, A.F. Hollenkamp, Emerging electrochemical energy conversion and storage technologies, Front. Chem. 2 (2014) 1–28, https://doi.org/10.3389/fchem.2014.00079.

[66] N. Li, K. Tong, L. Yang, X. Du, Review of 3D printing in photocatalytic substrates and catalysts, Mater. Today Energy 29 (2022) 101100, https://doi.org/10.1016/j.mtener.2022.101100.

[67] M.Z. Hussain, P.F. Großmann, F. Kohler, T. Kratky, L. Kronthaler, B. van der Linden, K. Rodewald, B. Rieger, R.A. Fischer, Y. Xia, 3D-Printed metal–organic framework-derived composites for enhanced photocatalytic hydrogen generation, Sol. RRL 6 (2022), https://doi.org/10.1002/solr.202200552.

[68] S. Lawson, K. Baamran, K. Newport, F. Rezaei, A. Rownaghi, Screening of adsorbent/catalyst composite monoliths for carbon capture-utilization and ethylene production, ACS Appl. Mater. Interfaces 13 (2021) 55198–55207, https://doi.org/10.1021/acsami.1c17668.

[69] N. Uria, I. Ferrera, J. Mas, Electrochemical performance and microbial community profiles in microbial fuel cells in relation to electron transfer mechanisms, BMC Microbiol. 17 (2017) 1–12, https://doi.org/10.1186/s12866-017-1115-2.

[70] P. Theodosiou, J. Greenman, I.A. Ieropoulos, Developing 3D-printable cathode electrode for monolithically printed microbial fuel cells (MFCs), Molecules 25 (2020) 1–12, https://doi.org/10.3390/molecules25163635.

[71] J. You, H. Fan, J. Winfield, I.A. Ieropoulos, Complete microbial fuel cell fabrication using additive, Molecules 25 (2020) 1–12.

[72] E. Jannelli, P. Di Trolio, F. Flagiello, M. Minutillo, Development and performance analysis of biowaste based microbial fuel cells fabricated employing additive manufacturing technologies, Energy Proc. 148 (2018) 1135–1142, https://doi.org/10.1016/j.egypro.2018.08.029.

[73] M.C. Freyman, T. Kou, S. Wang, Y. Li, 3D printing of living bacteria electrode, Nano Res. 13 (2020) 1318–1323, https://doi.org/10.1007/s12274-019-2534-1.

[74] J. You, R.J. Preen, L. Bull, J. Greenman, I. Ieropoulos, 3D printed components of microbial fuel cells: towards monolithic microbial fuel cell fabrication using additive layer manufacturing, Sustain. Energy Technol. Assessments 19 (2017) 94–101, https://doi.org/10.1016/j.seta.2016.11.006.

[75] F. Baş, M.F. Kaya, 3D printed anode electrodes for microbial electrolysis cells, Fuel 317 (2022), https://doi.org/10.1016/j.fuel.2022.123560.

[76] A. Krige, U. Rova, P. Christakopoulos, 3D bioprinting on cathodes in microbial electrosynthesis for increased acetate production rate using Sporomusa ovata, J. Environ. Chem. Eng. 9 (2021) 106189, https://doi.org/10.1016/j.jece.2021.106189.

[77] K.C. Kwon, J.M. Suh, R.S. Varma, M. Shokouhimehr, H.W. Jang, Electrocatalytic water splitting and CO_2 reduction: sustainable solutions via single-atom catalysts supported on 2D materials, Small Methods 3 (2019) 1–20, https://doi.org/10.1002/smtd.201800492.

[78] M.G. Walter, E.L. Warren, J.R. McKone, S.W. Boettcher, Q. Mi, E.A. Santori, N.S. Lewis, Solar water splitting cells, Chem. Rev. 110 (2010) 6446–6473, https://doi.org/10.1021/cr1002326.

[79] J. Rupar, D. Tekić, A. Janošević Ležaić, K.K. Upadhyay, ORR catalysts derived from biopolymers, Catalysts 13 (2023), https://doi.org/10.3390/catal13010080.

[80] M.P. Browne, V. Urbanova, J. Plutnar, F. Novotný, M. Pumera, Inherent impurities in 3D-printed electrodes are responsible for catalysis towards water splitting, J. Mater. Chem. A 8 (2020) 1120–1126, https://doi.org/10.1039/c9ta11949c.

[81] D.M. Wirth, M.J. Sheaff, J.V. Waldman, M.P. Symcox, H.D. Whitehead, J.D. Sharp, J.R. Doerfler, A.A. Lamar, G. Leblanc, Electrolysis activation of fused-filament-fabrication 3D-printed electrodes for electrochemical and spectroelectrochemical analysis, Anal. Chem. 91 (2019) 5553–5557, https://doi.org/10.1021/acs.analchem.9b01331.

[82] K. Ghosh, S. Ng, C. Iffelsberger, M. Pumera, 2D MoS_2/carbon/polylactic acid filament for 3D printing: photo and electrochemical energy conversion and storage, Appl. Mater. Today 26 (2022) 101301, https://doi.org/10.1016/j.apmt.2021.101301.

[83] S. Ng, R. Zazpe, J. Rodriguez-Pereira, J. Michalička, J.M. Macak, M. Pumera, Atomic layer deposition of photoelectrocatalytic material on 3D-printed nanocarbon structures, J. Mater. Chem. A 9 (2021) 11405–11414, https://doi.org/10.1039/d1ta01467f.

[84] C.W. Foster, M.P. Down, Y. Zhang, X. Ji, S.J. Rowley-Neale, G.C. Smith, P.J. Kelly, C.E. Banks, 3D printed graphene based energy storage devices, Sci. Rep. 7 (2017) 1–11, https://doi.org/10.1038/srep42233.

[85] J. Ahn, Y.S. Park, S. Lee, J. Yang, J. Pyo, J. Lee, G.H. Kim, S.M. Choi, S.K. Seol, 3D-printed NiFe-layered double hydroxide pyramid electrodes for enhanced electrocatalytic oxygen evolution reaction, Sci. Rep. 12 (2022) 1–10, https://doi.org/10.1038/s41598-021-04347-9.

[86] J. Ahn, S. Lee, J.H. Kim, M. Wajahat, H.H. Sim, J. Bae, J. Pyo, M. Jahandar, D.C. Lim, S.K. Seol, 3D-printed Cu_2O photoelectrodes for photoelectrochemical water splitting, Nanoscale Adv. 2 (2020) 5600–5606, https://doi.org/10.1039/d0na00512f.

[87] S. Chandrasekaran, J. Feaster, J. Ynzunza, F. Li, X. Wang, A.J. Nelson, M.A. Worsley, Three-dimensional printed MoS_2/graphene aerogel electrodes for hydrogen evolution reactions, ACS Mater. Au (2022), https://doi.org/10.1021/acsmaterialsau.2c00014.

[88] C. Iffelsberger, D. Rojas, M. Pumera, Photo-responsive doped 3D-printed copper electrodes for water splitting: refractory one-pot doping dramatically enhances the performance, J. Phys. Chem. C 126 (2022) 9016–9026, https://doi.org/10.1021/acs.jpcc.1c10686.

[89] B. Hüner, N. Demir, M.F. Kaya, Ni-Pt coating on graphene based 3D printed electrodes for hydrogen evolution reactions in alkaline media, Fuel 331 (2023) 125971, https://doi.org/10.1016/j.fuel.2022.125971.

[90] E. Vaněčková, M. Bouša, Š. Nováková Lachmanová, J. Rathouský, M. Gál, T. Sebechlebská, V. Kolivoška, 3D printed polylactic acid/carbon black electrodes with nearly ideal electrochemical behaviour, J. Electroanal. Chem. 857 (2020), https://doi.org/10.1016/j.jelechem.2019.113745.

[91] S. Ates, E.B. Aydin, Fabrication of 3D-Printed Graphene/polylactic Acid and Carbon Nanofiber/Polylactic Acid Electrodes : New Solvent- Free Electrochemical Activation Method for Hydrogen Evolution Reactions, 2023, pp. 10–13, https://doi.org/10.1002/app.54348.

[92] B. Jiang, H. Huang, W. Gong, X. Gu, T. Liu, J. Zhang, W. Qin, H. Chen, Y. Jin, Z. Liang, L. Jiang, Wood-inspired binder enabled vertical 3D printing of g-C_3N_4/CNT arrays for highly efficient photoelectrochemical hydrogen evolution, Adv. Funct. Mater. x (2021), https://doi.org/10.1002/adfm.202105045.

[93] M. Hu, Y. Wang, D. Ye, A timely review of lithium-ion batteries in electric vehicles: progress, future opportunities, and challenges, E3S Web Conf. 308 (2021), https://doi.org/10.1051/e3sconf/202130801015.

[94] F. Schipper, D. Aurbach, A brief review: past, present and future of lithium ion batteries, Russ. J. Electrochem. 52 (2016) 1095–1121, https://doi.org/10.1134/S1023193516120120.

[95] N. Dhiman, V. Sharma, S. Ghosh, Perspective on biomass-based cotton-derived nanocarbon for multifunctional energy storage and harvesting applications, ACS Appl. Electron. Mater. (2023), https://doi.org/10.1021/acsaelm.3c00022.

[96] P. Xie, W. Yuan, X. Liu, Y. Peng, Y. Yin, Y. Li, Z. Wu, Advanced carbon nanomaterials for state-of-the-art flexible supercapacitors, Energy Storage Mater. 36 (2021) 56–76, https://doi.org/10.1016/j.ensm.2020.12.011.

[97] X. Peng, L. Peng, C. Wu, Y. Xie, Two dimensional nanomaterials for flexible supercapacitors, Chem. Soc. Rev. 43 (2014) 3303–3323, https://doi.org/10.1039/c3cs60407a.

[98] Y. Liu, R. Zhang, J. Wang, Y. Wang, Current and future lithium-ion battery manufacturing, iScience 24 (2021) 102332, https://doi.org/10.1016/j.isci.2021.102332.

[99] W. Yan, X. Cai, F. Tan, J. Liang, J. Zhao, C. Tan, 3D printing flexible zinc-ion microbatteries with ultrahigh areal capacity and energy density for wearable electronics, Chem. Commun. 59 (2023) 1661–1664, https://doi.org/10.1039/d2cc06777c.

[100] Y. Li, J. Qu, F. Li, Z. Qu, H. Tang, L. Liu, M. Zhu, O.G. Schmidt, Advanced architecture designs towards high-performance 3D microbatteries, Nano Mater. Sci. 3 (2021) 140–153, https://doi.org/10.1016/j.nanoms.2020.10.004.

[101] Y. Wang, K.S. Chen, J. Mishler, S.C. Cho, X.C. Adroher, A review of polymer electrolyte membrane fuel cells: technology, applications, and needs on fundamental research, Appl. Energy 88 (2011) 981–1007, https://doi.org/10.1016/j.apenergy.2010.09.030.

[102] M. Pei, H. Shi, F. Yao, S. Liang, Z. Xu, X. Pei, S. Wang, Y. Hu, 3D printing of advanced lithium batteries: a designing strategy of electrode/electrolyte architectures, J. Mater. Chem. A 9 (2021) 25237–25257, https://doi.org/10.1039/d1ta06683h.

[103] S. Tagliaferri, A. Panagiotopoulos, C. Mattevi, Direct ink writing of energy materials, Mater. Adv. 2 (2021) 540–563, https://doi.org/10.1039/d0ma00753f.

[104] J. Qian, Q. Chen, M. Hong, W. Xie, S. Jing, Y. Bao, G. Chen, Z. Pang, L. Hu, T. Li, Toward stretchable batteries: 3D-printed deformable electrodes and separator enabled by nanocellulose, Mater. Today 54 (2022) 18–26, https://doi.org/10.1016/j.mattod.2022.02.015.

[105] S. Dalwadi, A. Goel, C. Kapetanakis, D. Salas-de la Cruz, X. Hu, The integration of biopolymer-based materials for energy storage applications: a review, Int. J. Mol. Sci. 24 (2023), https://doi.org/10.3390/ijms24043975.

[106] H. Wang, P. Zheng, H. Yi, Y. Wang, Z. Yang, Z. Lei, Y. Chen, Y. Deng, C. Wang, Y. Yang, Low-cost and environmentally friendly biopolymer binders for Li-S batteries, Macromolecules 53 (2020) 8539–8547, https://doi.org/10.1021/acs.macromol.0c01576.

[107] K. Xu, N. Zhao, Y. Li, P. Wang, Z. Liu, Z. Chen, J. Shen, C. Liu, 3D printing of ultrathick natural graphite anodes for high-performance interdigitated three-dimensional lithium-ion batteries, Electrochem. Commun. 139 (2022) 107312, https://doi.org/10.1016/j.elecom.2022.107312.

[108] D. Vernardou, K.C. Vasilopoulos, G. Kenanakis, 3D printed graphene-based electrodes with high electrochemical performance, Appl. Phys. Mater. Sci. Process 123 (2017) 1–7, https://doi.org/10.1007/s00339-017-1238-1.

[109] C. Liu, F. Xu, X. Cheng, J. Tong, Y. Liu, Z. Chen, C. Lao, J. Ma, Comparative study on the electrochemical performance of $LiFePO_4$ cathodes fabricated by low temperature 3D printing, direct ink writing and conventional roller coating process, Ceram. Int. 45 (2019) 14188–14197, https://doi.org/10.1016/j.ceramint.2019.04.124.

[110] T. Xu, K. Liu, N. Sheng, M. Zhang, W. Liu, H. Liu, L. Dai, X. Zhang, C. Si, H. Du, K. Zhang, Biopolymer-based hydrogel electrolytes for advanced energy storage/conversion devices: properties, applications, and perspectives, Energy Storage Mater. (2022), https://doi.org/10.1016/j.ensm.2022.03.013.

[111] M. Cheng, Y. Jiang, 3D-printed solid-state electrolytes for electrochemical energy storage devices, J. Mater. Res. 36 (2021) 4547–4564, https://doi.org/10.1557/s43578-021-00355-7.

[112] P. Bao, Y. Lu, P. Tao, B. Liu, J. Li, X. Cui, 3D printing PEDOT-CMC-based high areal capacity electrodes for Li-ion batteries, Ionics 27 (2021) 2857–2865, https://doi.org/10.1007/s11581-021-04063-4.

[113] J. Huang, J. Yang, W. Li, W. Cai, Z. Jiang, Electrochemical properties of $LiCoO_2$ thin film electrode prepared by ink-jet printing technique, Thin Solid Films 516 (2008) 3314–3319, https://doi.org/10.1016/j.tsf.2007.09.039.

[114] I. Ben-Barak, Y. Kamir, S. Menkin, M. Goor, I. Shekhtman, T. Ripenbein, E. Galun, D. Golodnitsky, E. Peled, Drop-on-Demand 3D printing of lithium iron phosphate cathodes, J. Electrochem. Soc. 166 (2019) A5059–A5064, https://doi.org/10.1149/2.0091903jes.

[115] C. Milroy, A. Manthiram, Printed microelectrodes for scalable, high-areal-capacity lithium-sulfur batteries, Chem. Commun. 52 (2016) 4282–4285, https://doi.org/10.1039/c5cc10503j.

[116] H. Ragones, S. Menkin, Y. Kamir, A. Gladkikh, T. Mukra, G. Kosa, D. Golodnitsky, Towards smart free form-factor 3D printable batteries, Sustain. Energy Fuels 2 (2018) 1542–1549, https://doi.org/10.1039/c8se00122g.

[117] G. Shi, X. Peng, J. Zeng, L. Zhong, Y. Sun, W. Yang, Y.L. Zhong, Y. Zhu, R. Zou, S. Admassie, Z. Liu, C. Liu, E.I. Iwuoha, J. Lu, A liquid metal microdroplets initialized hemicellulose composite for 3D printing anode host in Zn-ion battery, Adv. Mater. (2023) 2300109, https://doi.org/10.1002/adma.202300109, 1–10.

[118] W. Gao, C. Iffelsberger, M. Pumera, Dual polymer engineering enables high-performance 3D printed Zn-organic battery cathodes, Appl. Mater. Today 28 (2022) 101515, https://doi.org/10.1016/j.apmt.2022.101515.

[119] A.A. Kebede, T. Kalogiannis, J. Van Mierlo, M. Berecibar, A comprehensive review of stationary energy storage devices for large scale renewable energy sources grid integration, Renew. Sustain. Energy Rev. 159 (2022) 112213, https://doi.org/10.1016/j.rser.2022.112213.

[120] A. Tanwilaisiri, Y. Xu, R. Zhang, D. Harrison, J. Fyson, M. Areir, Design and fabrication of modular supercapacitors using 3D printing, J. Energy Storage 16 (2018) 1–7, https://doi.org/10.1016/j.est.2017.12.020.

[121] L.S. Anthony, M. Vasudevan, V. Perumal, M. Ovinis, P.B. Raja, T.N.J.I. Edison, Bioresource-derived polymer composites for energy storage applications: brief review, J. Environ. Chem. Eng. 9 (2021) 105832, https://doi.org/10.1016/j.jece.2021.105832.

[122] Z. Huang, H. Zhang, M. Guo, M. Zhao, Y. Liu, D. Zhang, M. Terrones, Y. Wang, Large-scale preparation of electrically conducting cellulose nanofiber/carbon nanotube aerogels: ambient-dried, recyclable, and 3D-Printable, Carbon N. Y. 194 (2022) 23–33, https://doi.org/10.1016/j.carbon.2022.03.056.

[123] X. Aeby, A. Poulin, G. Siqueira, M.K. Hausmann, G. Nyström, Fully 3D printed and disposable paper supercapacitors, Adv. Mater. (2021) 2101328, https://doi.org/10.1002/adma.202101328, 1–9.

[124] G. Zhou, M.C. Li, C. Liu, Q. Wu, C. Mei, 3D printed $Ti_3C_2T_x$ MXene/cellulose nanofiber architectures for solid-state supercapacitors: ink rheology, 3D printability, and electrochemical performance, Adv. Funct. Mater. (2021) 2109593, https://doi.org/10.1002/adfm.202109593, 1–11.

[125] V. Krishnadoss, B. Kanjilal, A. Masoumi, A. Banerjee, Programmable bio-ionic liquid functionalized hydrogels for in situ 3D bioprinting of electronics at the tissue interface, Mater. Today Adv. 17 (2023) 100352, https://doi.org/10.1016/j.mtadv.2023.100352.

[126] V. Krishnadoss, B. Kanjilal, A. Hesketh, C. Miller, A. Mugweru, M. Akbard, A. Khademhosseini, I. Noshadi, In situ 3D printing of implantable energy storage devices, Chem. Eng. J. 409 (2021) 128213, https://doi.org/10.1016/j.cej.2020.128213.

[127] W. Zong, Y. Ouyang, Y. Miao, Recent Advances and Perspectives of 3D Printed Micro-supercapacitors : from Design to Smart, 2022, pp. 2075–2095, https://doi.org/10.1039/d1cc05544e.

[128] H. Li, J. Liang, Recent development of printed micro-supercapacitors : printable materials, Printing Technol. Perspect. (2020) 1805864, https://doi.org/10.1002/adma.201805864, 1–19.

[129] Y. Zhang, Y. Song, Y. Shi, Y. Wang, X. Wang, X. Shi, C. Tang, J. Liu, G. Wang, Q. Tan, L. Li, Applied surface science high-performance all-solid-state microsupercapacitors from 3D printing structure-engineered graphene-carbon sphere electrodes, Appl. Surf. Sci. 597 (2022) 153730, https://doi.org/10.1016/j.apsusc.2022.153730.

[130] Z. Yang, X. Lv, C. Zhang, Y. Zhang, S. Jia, Y. Niu, Y. Zhang, B. Wang, T. Zhao, H. Fu, Q. Li, Core-sheath 3D printing of highly conductive and MoS_2-loaded electrode with pseudocapacitive behavior, Chem. Eng. J. 423 (2021) 130304, https://doi.org/10.1016/j.cej.2021.130304.
[131] M. Zhang, M. Zhao, M. Jian, C. Wang, A. Yu, Z. Yin, X. Liang, H. Wang, K. Xia, X. Liang, J. Zhai, Y. Zhang, Printable smart pattern for multifunctional energy-management E-textile, Matter 1 (2019) 168–179, https://doi.org/10.1016/j.matt.2019.02.003.
[132] W. Kang, L. Zeng, S. Ling, C. Zhang, 3D printed supercapacitors toward trinity excellence in kinetics, energy density, and flexibility, Adv. Energy Mater. 11 (2021) 1–10, https://doi.org/10.1002/aenm.202100020.
[133] W. Gao, C. Iffelsberger, M. Pumera, Dual polymer engineering enables high-performance 3D printed Zn-organic battery cathodes, Appl. Mater. Today 28 (2022) 101515, https://doi.org/10.1016/j.apmt.2022.101515.
[134] B. Yao, H. Peng, H. Zhang, J. Kang, C. Zhu, G. Delgado, D. Byrne, S. Faulkner, M. Freyman, X. Lu, M.A. Worsley, J.Q. Lu, Y. Li, Printing porous carbon aerogels for low temperature supercapacitors, Nano Lett. 21 (2021) 3731–3737, https://doi.org/10.1021/acs.nanolett.0c04780.
[135] K. Ghosh, S. Ng, C. Iffelsberger, M. Pumera, Inherent impurities in graphene/polylactic acid filament strongly influence on the capacitive performance of 3D-printed electrode, Chem. Eur J. 26 (2020) 15746–15753, https://doi.org/10.1002/chem.202004250.
[136] Q. Yang, Zhengpeng, Xinyin Yang, Tingting Yang, Yufang Cao, Chunjing Zhang, Yongyi Zhang, Ping Li, Junfei Yang, Yuyan Ma, Li, 3D printing of carbon tile-modulated well-interconnected hierarchically porpous pseudocapacitive electrode, 2022, pp. 6–11, 2.
[137] Y. Zhang, W. Peng, Y. Cao, W. Wang, D. Teng, Y. Huang, G. Fan, 3D graphene-based active electrodes with large areal capacitance by modified direct ink writing method colloids and surfaces A : physicochemical and engineering aspects 3D graphene-based active electrodes with large areal capacitance by modified direct in, Colloids Surf. A Physicochem. Eng. Asp. 671 (2023) 131603, https://doi.org/10.1016/j.colsurfa.2023.131603.
[138] Q. Wang, X. Liu, Z. Qiang, Z. Hu, X. Cui, H. Wei, J. Hu, Y. Xia, S. Huang, J. Zhang, K. Fu, Y. Chen, Cellulose nanocrystal enhanced, high dielectric 3D printing composite resin for energy applications, Compos. Sci. Technol. 227 (2022) 109601, https://doi.org/10.1016/j.compscitech.2022.109601.
[139] F. Wang, Y. Deng, C. Yuan, Design and cost modeling of high capacity lithium ion batteries for electric vehicles through a techno-economic analysis approach, Procedia Manuf. 49 (2020) 24–31, https://doi.org/10.1016/j.promfg.2020.06.006.
[140] E. Karayel, Y. Bozkurt, Additive manufacturing method and different welding applications, J. Mater. Res. Technol. 9 (2020) 11424–11438, https://doi.org/10.1016/j.jmrt.2020.08.039.
[141] J. Bae, S. Kim, J. Ahn, H.H. Sim, M. Wajahat, J.H. Kim, S. Yoon, J.T. Kim, S.K. Seol, J. Pyo, Nanoscale 3D printing of quantum dots on paper, Adv. Eng. Mater. (2021) 2100339, https://doi.org/10.1002/adem.202100339, 1–6.
[142] T.G. Pattison, S. Wang, R.D. Miller, G. yu Liu, G.G. Qiao, 3D nanoprinting via spatially controlled assembly and polymerization, Nat. Commun. 13 (2022) 1–7, https://doi.org/10.1038/s41467-022-29432-z.
[143] M.R. Penny, S.T. Hilton, Design and development of 3D printed catalytically-active stirrers for chemical synthesis, React. Chem. Eng. 5 (2020) 853–858, https://doi.org/10.1039/c9re00492k.
[144] S.S. Mahdavi, M.J. Abdekhodaie, H. Kumar, S. Mashayekhan, A. Baradaran-Rafii, K. Kim, Stereolithography 3D bioprinting method for fabrication of human corneal stroma equivalent, Ann. Biomed. Eng. 48 (2020) 1955–1970, https://doi.org/10.1007/s10439-020-02537-6.
[145] M.M. Sk, P. Das, A. Panwar, L.P. Tan, Synthesis and characterization of site selective photo-crosslinkable glycidyl methacrylate functionalized gelatin-based 3D hydrogel scaffold for liver tissue engineering, Mater. Sci. Eng. C 123 (2021) 111694, https://doi.org/10.1016/j.msec.2020.111694.
[146] V.B. Morris, S. Nimbalkar, M. Younesi, P. McClellan, O. Akkus, Mechanical properties, cytocompatibility and manufacturability of chitosan:PEGDA hybrid-gel scaffolds by stereolithography, Ann. Biomed. Eng. 45 (2017) 286–296, https://doi.org/10.1007/s10439-016-1643-1.
[147] I. Koumentakou, M.J. Noordam, A. Michopoulou, Z. Terzopoulou, D.N. Bikiaris, 3D-Printed chitosan-based hydrogels loaded with levofloxacin for tissue engineering applications, Biomacromolecules 24 (2023) 4019–4032, https://doi.org/10.1021/acs.biomac.3c00362.
[148] L. Zhou, H. Ramezani, M. Sun, M. Xie, J. Nie, S. Lv, J. Cai, J. Fu, Y. He, 3D printing of high-strength chitosan hydrogel scaffolds without any organic solvents, Biomater. Sci. 8 (2020) 5020–5028, https://doi.org/10.1039/d0bm00896f.